Western Blot Analysis

Wild-type and *Il-6*KO fibroblasts were prepared as described above and cultured to semiconfluence in 100-cm^2 culture plates. Before treatment, fibroblast cultures were washed twice with PBS, and culture media were replaced with low-serum (0.1%fetal bovine serum) Dulbecco's modified Eagle's medium containing 60 IU/mL *penicillin*, 100 IU/mL *streptomycin*, and 4 *mmol/L glutamine*. Low-serum medium was necessary to maintain viability of primary fibroblasts overnight.

Following 12 hours incubation in low-serum medium, treatments were applied to the cultures in fresh low-serum Dulbecco's modified Eagle's medium. Semiconfluent cultures were treated with 10 ng/mL of MR16-1 or 10 μmol/L of PD98058 (Calbiochem, San Diego, CA) for 3 hours, and then 10 ng/mL of recombinant mouse IL-6 (R&D Systems, Minneapolis, MN) was added to the cultures for 24 hours. At indicated time points, culture plates were rinsed twice with ice-cold PBS, and total cell protein was collected in 500 μL of lysis buffer [50 mmol/L Tris-HCl (pH 7.6), 150 mmol/L NaCl, 1% deoxycholic acid, 0.1% sodium dodecyl sulfate, 1% Triton X-100, 1 mmol/L sodium orthovanadate, and protease inhibitor cocktail]. Western blot analysis was performed as previously described.[4] Ten micrograms of protein were fractionated on SDS-polyacrylamide gels and transferred onto PVDF membranes (Bio-Rad, Hercules, CA). Nonspecific protein binding was blocked by incubating the membranes in 5% w/v nonfat milk powder in TBST [50 mmol/L Tris-HCl (pH 7.6), 150 mmol/L NaCl, and 0.1% v/v Tween-20]. The membranes were incubated with mouse monoclonal anti-α-SMA (Dako-Cytomation) Ab at a dilution of 1:1000 overnight at 4°C or with *mouse monoclonal anti-β-actin (Sigma-Aldrich)* at a dilution of 1:5000 for 30 minutes at room temperature. After three 5-minute washes in TBST, membranes were incubated with horseradish peroxidase–conjugated anti-mouse Ab at a dilution of 1:10,000 for 60 minutes at room temperature. Protein bands were detected using the ECL Plus kit (GE Healthcare, Little Chalfont, UK). Western blot quantification was performed with ImageJ software (NIH, Bethesda, MD) and used to visualize fold expression differences between these treatment groups.

Mice and Induction of Skin Sclerosis

Six-week-old female mice were used in all experiments. C57BL/6 mice were purchased from Japan Clea (Osaka, Japan). Mutant C57BL/6 mice rendered null for IL-6 were *described previously*[17] and were purchased from the National Institute of Biomedical Innovation (Osaka, Japan). Mice were maintained in our pathogen-free animal facility. All animal care was in accordance with the institutional guidelines of Osaka University. BLM (Nippon Kayaku, Tokyo, Japan) was dissolved in PBS at a concentration of 1 mg/mL and sterilized by filtration. BLM (0.1 *mg*/100 μL) was *injected subcutaneously into* the shaved back of the mice daily for 4 weeks with a 27-gauge needle as described by Yamamoto et al.[7] Control mice received 100 μL of PBS instead.

RNA Isolation and Real-Time PCR

Sections of skin lesions and the cutaneous draining lymph nodes (LNs) were removed 1 day after the final injection. Total RNA was isolated using the SV Total RNA Isolation System (Promega, Madison, WI) and reverse transcribed into complementary DNA.

IL-6 expression was measured using the Power SYBR Green PCR Master Mix (Applied Biosystems, Foster City, CA) *according to the manufacturer's protocol*. Glyceraldehyde-3-phosphate dehydrogenase (GAPDH) was used to normalize the mRNA. Sequence-specific primers were: IL-6, sense 5′-ACACACTGGTTCTGAGGGAC-3′, antisense 5′-TACCACAAGGTTGGCAGGTG-3′; GAPDH, sense 5′-TGTCATCATACTTGGCAGGTTTCT-3′, antisense 5′-CATGGCCTTCCGTGTTCCTA-3′. Real-time PCR (40 cycles of denaturing at 92°C for 15 seconds and annealing at 60°C for 60 seconds) was run on an ABI 7000 Prism Detection System (Applied Biosystems).

Table 1. *Continued*

α-SMA–Positive Cells (Cells/HPS)			Mast Cells (Cells/HPS)		
1st (n = 4)	2nd (n = 4)	3rd (n = 4)	1st (n = 4)	2nd (n = 4)	3rd (n = 4)
6.00 ± 4.08	3.50 ± 1.29	8.75 ± 1.50	12.50 ± 4.51	21.67 ± 3.06	31.50 ± 5.45
5.00 ± 1.73	4.00 ± 1.41	10.00 ± 4.16	11.00 ± 1.83	17.33 ± 6.11	29.75 ± 3.50
83.33	114.29	114.29	88.00	80.00	94.44
	104.0 ± 10.32			87.48 ± 4.177	
14.00 ± 1.83*	14.50 ± 4.93*	27.75 ± 0.96*	46.50 ± 8.43*	35.33 ± 5.69*	67.25 ± 5.85*
10.00 ± 1.41	7.00 ± 1.82§	15.25 ± 2.75†	20.25 ± 4.99†	25.00 ± 2.00	29.50 ± 6.19†
71.43	48.28	54.95	43.55	70.75	43.87
	58.22 ± 6.88			52.72 ± 9.02	

Table 2. Effect of MR16-1 on BLM-Induced Dermal Sclerosis in a Treatment Model

	Thickness (mm)		Hardness (arbitrary)		α-SMA–positive cells (cells/HPS)		Mast cells (cells/HPS)	
	1st (n = 4)	2nd (n = 3)	1st (n = 4)	2nd (n = 3)	1st (n = 4)	2nd (n = 3)	1st (n = 4)	2nd (n = 3)
PBS								
Control Ab	0.14 ± 0.02	0.12 ± 0.03	4.80 ± 0.47	6.19 ± 1.29	3.75 ± 1.50	2.33 ± 0.58	13.50 ± 1.73	19.67 ± 2.52
MR16-1	0.12 ± 0.01	0.107 ± 0.006	4.67 ± 0.47	5.68 ± 0.43	3.33 ± 0.56	2.67 ± 1.15	15.33 ± 1.15	21.00 ± 2.00
% Changes	83.64	86.49	97.22	91.78	88.88	106.78	113.58	106.78
BLM								
Control Ab	0.30 ± 0.03*	0.29 ± 0.03*	9.34 ± 1.58*	9.81 ± 1.17†	10.00 ± 2.58*	7.67 ± 0.58*	37.75 ± 2.50*	54.67 ± 8.39*
MR16-1	0.21 ± 0.05‡∥	0.18 ± 0.03§¶	5.46 ± 0.62¶	5.41 ± 0.77¶	5.50 ± 1.29¶	4.00 ± 1.00¶	27.00 ± 2.16*¶	37.00 ± 6.56‡∥
% Changes	70.00	62.50	58.46	55.12	55.00	52.17	71.52	67.68

Mean ± SD is presented. To quantify the impact of MR16-1treatment, % changes were calculated as follows (evaluative consequences of MR16-1 treatment/that of PBS treatment) × 100 (%)
*P < 0.01 PBS+Control Ab versus BLM+Cont. Ab.
†P < 0.05 PBS+Control Ab versus BLM+Cont. Ab
‡P < 0.05 BLM+Control Ab versus BLM+MR16-1
§P < 0.01 PBS+MR16-1 versus BLM+MR16-1
¶P < 0.01 BLM+Control Ab versus BLM+MR16-1
∥P < 0.05 PBS+MR16-1 versus BLM+MR16-1
HPS, high-power field

Mouse IL-6 Receptor–Specific Monoclonal Antibody Treatment

Rat anti-mouse IL-6 receptor monoclonal Ab (clone MR16-1, *rat* IgG_1, *described previously*[18] was *provided* by Chugai Pharmaceutical (Shizuoka, Japan). Purified rat IgG_1 (isotype-matched control Ab) (Cappel, MP Biomedicals, Solon, OH) was administered as a control. Preventive and therapeutic administration methods are discussed later. Percentage to control values were calculated as follows: (mean actual value/mean control value) × 100.

Enzyme-Linked Immunosorbent Assay of IL-6 Levels in Sera and Conditioned Media

Serum samples were obtained from mice injected with BLM or PBS for 28 days. *Conditioned media* were obtained from cultured primary dermal fibroblasts of wild-type and *Il-6*KO mice after 24 hours. Serum and conditioned media IL-6 level was measured by enzyme-linked immunosorbent assay using a commercial kit (R&D Systems, Minneapolis, MN) with a detection limit of 7.8 pg/mL.

Vesmeter Measurements

Skin hardness was measured using a Vesmeter.[19] Mice were sacrificed 1 day after the final injection. Skin hardness was measured three times at the injection area, avoiding the backbone of the mouse. Skin hardness was expressed as the area of the depression caused by the

Table 3. Attenuated BLM-Induced Dermal Sclerosis in *Il-6*KO Mice

	Thickness (mm)		Hardness (arbitrary)		α-SMA–positive cells (cells/HPS)		Mast cells (cells/HPS)	
	1st (n = 4)	2nd (n = 3)	1st (n = 4)	2nd (n = 3)	1st (n = 4)	2nd (n = 3)	1st (n = 4)	2nd (n = 3)
WT								
PBS	0.112 ± 0.013	0.14 ± 0.04	4.91 ± 0.38	5.46 ± 0.93	4.75 ± 1.50	8.00 ± 2.00	18.00 ± 3.16	28.33 ± 4.51
BLM	0.32 ± 0.02*	0.29 ± 0.06†	12.38 ± 0.81*	9.69 ± 0.51*	19.75 ± 5.74*	23.33 ± 6.11*	40.25 ± 2.22*	63.33 ± 9.87*
% Change	282.85	203.13	251.99	177.28	415.79	291.67	223.61	223.53
Il-6								
PBS	0.111 ± 0.010	0.12 ± 0.01	5.37 ± 0.48	5.12 ± 0.71	4.00 ± 1.41	6.67 ± 2.52	17.75 ± 2.5	29.5 ± 0.71
BLM	0.22 ± 0.03†§	0.17 ± 0.03‡	7.14 ± 0.96‡¶	5.85 ± 0.21†	9.50 ± 4.43∥	13.00 ± 1.73∥	22.75 ± 4.79‡	34.00 ± 7.00∥
% Change	195.71	133.81	132.87	114.21	237.50	195.00	128.17	115.25

Mean ± SD was presented. To quantify the impact of BLM treatment, % changes were calculated as follows (evaluative consequences of BLM treatment/that of PBS treatment) × 100 (%)
*P < 0.01 WT with PBS versus WT with BLM.
†P < 0.05 WT with PBS versus WT with BLM.
‡P < 0.01 WT with BLM versus *Il-6*KO with BLM.
§P < 0.01 *Il-6*KO with PBS versus *Il-6*KO with BLM.
¶P < 0.05 *Il-6*KO with PBS versus *Il-6*KO with BLM.
∥P < 0.05 WT with BLM versus *Il-6*KO with BLM.
HPS, high-power field; WT, wild-type.

Table 4. Number of Lymph Node Cells in the Scleroderma Mouse Model

	1st experiment (total number/lymph node, × 10^7)			2nd experiment (total number/lymph node, × 10^6)		
	PBS	BLM	% Change	PBS	BLM	% Change
WT						
Control Ab	0.97 ± 0.21 (n = 3)	2.17 ± 0.31* (n = 3)	222.61	1.90 ± 0.41 (n = 4)	3.55 ± 0.21* (n = 4)	186.73
MR16-1	0.76 ± 0.02 (n = 3)	0.80 ± 0.12† (n = 3)	105.29	1.85 ± 0.18 (n = 4)	1.85 ± 0.34† (n = 4)	99.84
Il-6KO						
WT	0.81 ± 0.18 (n = 3)	1.53 ± 0.40‡ (n = 3)	190.03	2.36 ± 0.26 (n = 3)	3.71 ± 0.61‡ (n = 3)	157.42
Il-6KO	0.66 ± 0.26 (n = 3)	0.54 ± 0.09§ (n = 3)	82.73	1.97 ± 0.67 (n = 3)	2.20 ± 0.29§ (n = 3)	111.51

Mean ± SD was presented. To quantify the impact of BLM treatment, % changes were calculated as follows: (evaluative consequences of BLM treatment/that of PBS treatment) × 100 (%).
*$P < 0.01$ PBS+Control Ab versus BLM+Cont. Ab.
†$P < 0.01$ BLM+Control Ab versus BLM+MR16-1.
‡$P < 0.05$ PBS+Control Ab versus BLM+Cont. Ab.
§$P < 0.05$ BLM+Control Ab versus BLM+MR16-1.

probe divided by the pressure of the indenter in a connected computer.

Histopathological Analysis

The back skin was removed 1 day after the final injection. Skin pieces were fixed with 10% formaldehyde for 24 hours, embedded in paraffin, and sectioned at 3-μm thickness using a microtome. Sections were stained with hematoxylin and eosin (H&E). Dermal thickness (measured from the epidermal–dermal junction to dermal–fat junction) was determined at ×100 magnification at three randomly selected sites in each animal. Mast cells were identified in 3-μm deparaffinized sections stained with 1% Toluidine Blue, and mast cells were counted in 10 randomly selected sites under × 400 power using light microscopy.

Immunohistochemical Analysis of α-SMA

Sections were cut and processed as described above. For immunohistochemical analysis, sections were deparaffinized by passage through xylene and graded ethanols. Next, endogenous peroxide was blocked using 3% H_2O_2 in methanol for 5 minutes. Slides were blocked with 2% bovine serum albumin for 10 minutes, and stained with primary Ab (anti–α-SMA Ab 1:100 dilution) for 60 minutes. After washing with PBS containing 0.05% Triton, they were developed using Dako ChemMate Envision Kit/horseradish peroxidase (Dako-Cytomation) for 30 minutes, and counterstained with hematoxylin. α-SMA–positive fibroblastic cells were counted in 10 randomly selected sites under × 400 power using light microscopy.

Flow Cytometric Analysis

The skin draining LNs were assessed as a mixture to facilitate analysis. One day after the final infection, mice were sacrificed, and axillary, brachial, and inguinal LNs from each mouse were combined. Cell suspensions of LN cells were stained with antibodies against the following cell surface antigens: CD4, CD8, B220, CD11c, F4/80, and PDCA1 (BD Biosciences, San Jose, CA). Stained cells were analyzed by flow cytometry using a FACSCalibur flow cytometer (BD Biosciences).

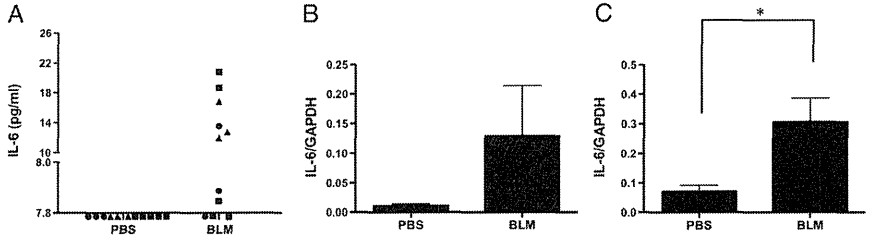

Figure 1. IL-6 production in BLM-treated C57BL/6 mice. C57BL/6 mice treated with PBS or BLM for 4 weeks. **A:** Serum samples were obtained from mice injected with 1 mg/mL BLM (100 μL/day, n = 11) or PBS (100 μL/day, n = 11) for 4 weeks. The data presented are from three experiments of three to five mice each for a total of 11 BLM-treated mice and 11 PBS-treated mice. Serum IL-6 level was measured by enzyme-linked immunosorbent assay using a kit with a detection limit of 7.8 pg/mL (R&D Systems). The mice from different experiments were gave different symbols [box (n = 5), circle (n = 3), and triangles (n = 3)]. Each symbol represents one IL-6 measurement for a single mouse, and symbols below 7.8 pg/mL indicate mice for which IL-6 was below the limit of detection. enzyme-linked immunosorbent assays were run in duplicate for all mice, with similar results. **B** and **C:** Expression of IL-6 mRNA was measured by real-time PCR. RNA was extracted from skin lesions (**B**) and cutaneous draining LNs (**C**) from C57BL/6 mice treated with PBS (n = 3) or BLM (n = 3) for 4 weeks. Data were normalized to the GAPDH internal control. Bars represent mean ± SD. *$P < 0.05$, unpaired t-test. Data in B and C are from one of two independent experiments that gave similar results. The IL-6/GAPDH data (mean ± SD) for skin lesions (**B**) were as follows: first experiment (n = 3), PBS: 0.011 ± 0.006, BLM: 0.129 ± 0.148 (P = 0.2391); second experiment (n = 3), PBS: 0.142 ± 0.070, BLM: 0.441 ± 0.283 (P = 0.1495). The IL-6/GAPDH data (mean ± SD) for cutaneous draining LNs (**C**) were as follows: first experiment (n = 3), PBS: 0.071 ± 0.038, BLM: 0.306 ± 0.141 (P = 0.0493), second experiment (n = 3), PBS: 0.083 ± 0.0.067, BLM: 0.430 ± 0.175 (P = 0.0521).

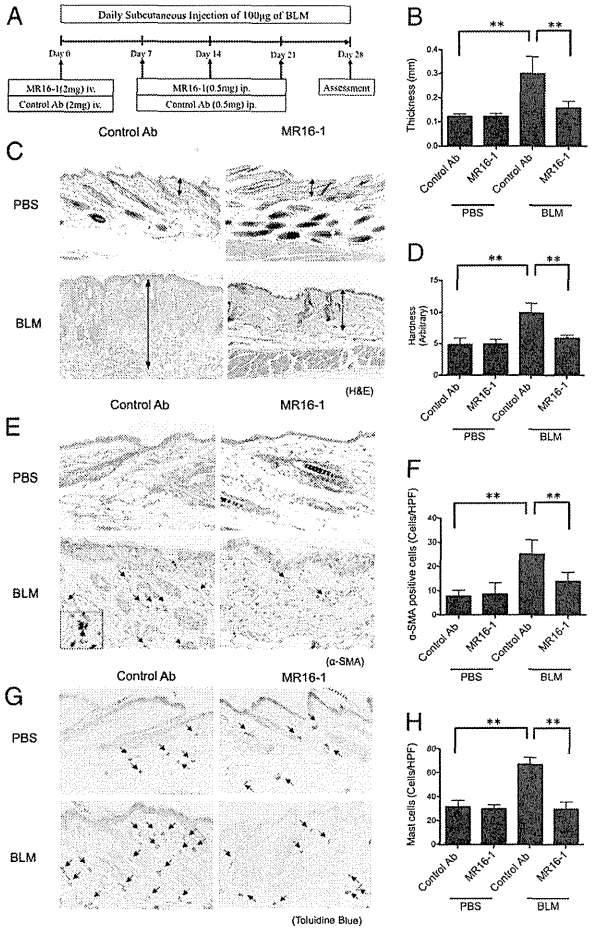

Figure 2. Effect of MR16-1 on BLM-induced dermal sclerosis in a prevention model. **A:** Experimental protocol for prevention of BLM-induced dermal sclerosis by administration of MR16-1 or control Ab to either PBS- or BLM-treated mice (n = 4 for each group). Histological and physical examination of the lesional skin was performed on the final day (day 28) of the protocol. **B:** Measurements of dermal thickness (n = 4 for each group). **C:** H&E staining of specimens derived from PBS-, or BLM-injected mice treated with MR16-1 or control Ab (original magnification, ×40). The length of each **two-headed arrow** indicates the measurement region of dermal thickness. **D:** Skin hardness measurements obtained using a Vesmeter (n = 4 for each group). **E:** Immunohistochemical staining for α-SMA. **Arrows** indicate α-SMA–positive fibroblasts (original magnification, ×100). **Inset** photo shows higher magnification (×200) of α-SMA–positive fibroblasts. **F:** The number of α-SMA–positive fibroblasts per high-power field (HPF, ×400) was determined by observation of 10 random grids. The value graphed is the average of the observation of 10 grids for each of the four mice in the group. **G:** Results of Toluidine Blue staining. **Arrows** indicate the metachromatically stained mast cells (original magnification, ×100). **H:** The number of mast cells per HPF (×400) was determined by observation of 10 random grids. The value graphed is the average of the observation of 10 grids for each of the four mice in the group. **C**, **D**, **F**, and **H:** Bars represent mean ± SD. *$P < 0.05$, **$P < 0.01$, one-way analysis of variance and Bonferroni post hoc multiple comparison. Data presented are from the third of three independent experiments with similar results presented in Table 1.

Computation Methods and Statistical Analysis

All data except change ratios are expressed as mean values ± standard deviations (SDs). To quantify the impact of MR16-1-and BLM treatment, change ratios (%) are calculated for single experiments in Table 1–4. Percent changes in Table 1 are averaged for three experiments and expressed as mean values ± standard errors (SEs). Unpaired t-test was used to examine the statistical value between two variable quantities. One-way analysis of variance and the Bonferroni post hoc multiple comparison procedure were used to determine the level of significance between each of three or more variable quantities.

Results

Elevated IL-6 in Mice with BLM-Induced Scleroderma

We first determined the serum concentration and mRNA expression of IL-6 in the skin and cutaneous draining LNs from mice with skin fibrosis induced by subcutaneous

BLM injection. Serum IL-6 levels were undetectable by enzyme-linked immunosorbent assay in all PBS-treated mice, and in 3 of 11 C57BL/6 mice treated with BLM. However, IL-6 was detectable, thus elevated, in 8 of 11 BLM-treated mice (Figure 1A), with a mean of 11.9 ± 5.24 pg/mL (n = 8). IL-6 mRNA expression showed a trend toward increased levels in the skin of mice treated with BLM that was not statistically significant (Figure 1B), and was significantly elevated ($P < 0.05$) in the cutaneous draining LNs of BLM-treated mice relative to PBS-treated mice (Figure 1C). These results are consistent with a role for IL-6 in the pathogenesis of scleroderma in the BLM-induced mouse model.

MR16-1 Prevents BLM-Induced Dermal Sclerosis

We next investigated whether MR16-1, a rat anti-mouse IL-6 receptor monoclonal Ab, could ameliorate the dermal thickening and skin hardening symptoms observed in BLM-treated mice. Figure 2A shows the administration schedule of preventive intervention. Dermal thickness was significantly increased at the BLM injection site of control Ab–treated mice, but nearly normal at the PBS injection site of control Ab–, or MR16-1–treated mice. Importantly, BLM-induced dermal thickening was significantly attenuated by prophylactic administration of MR16-1 (Figure 2, B and C, Table 1).

Skin hardness in the BLM-injected group that was given MR16-1 was also significantly reduced compared to the BLM-injected group that was given the control Ab. The ameliorating effect of MR16-1 on skin hardness was relatively strong compared with the effect on dermal thickness (Figure 2, B and D, Table 1).

To further examine the effects of MR16-1 treatment, the numbers of α-SMA–positive fibroblasts (termed myofibroblasts) (Figure 2, E and F, Table 1) and mast cells (Figure 2, G and H, Table 1), both key players in sclerosis of skin lesions, were evaluated. The numbers of myofibroblasts and mast cells were significantly increased in BLM-injected mice treated with control Ab relative to PBS-injected mice treated with control Ab. In BLM-injected mice treated with MR16-1, the numbers of myofibroblasts and mast cells were decreased significantly compared to the control value (BLM-injected mice treated with control Ab) (Figure 2, E to H, Table 1). These results suggest that treatment with MR16-1 might be effective during the fibrosing phase of scleroderma.

MR16-1 Improves BLM-Induced Dermal Sclerosis

Figure 3A shows the administration schedule of treatment intervention. As expected, the dermal thickness and skin hardness induced by BLM were diminished by therapeutic administration of MR16-1 compared with control Ab (Figure 3, B to D). The numbers of myofibroblasts and mast cells in lesional skin were also decreased by administration of MR16-1 compared with control Ab (Figure 3, E and F). Table 2 summarizes the data from two treatment intervention experiments. These results indicate that IL-6 may contribute to the pathogenesis of BLM-induced scleroderma and that blockade of IL-6 receptor may be a novel treatment of scleroderma.

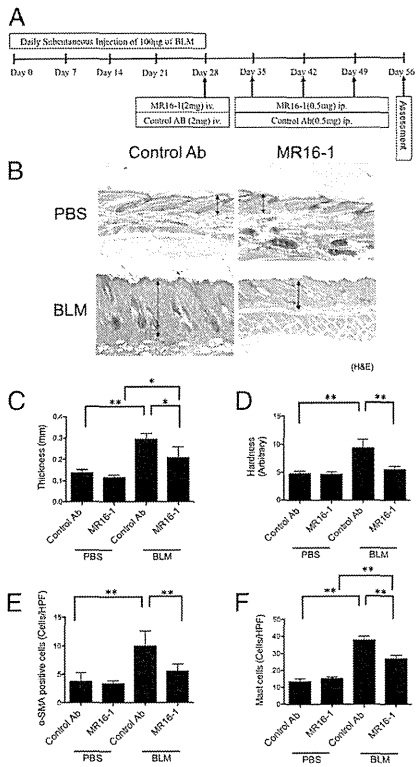

Figure 3. Effect of MR16-1 on BLM-induced dermal sclerosis in a treatment model. **A:** Experimental protocol for treatment of BLM-induced dermal sclerosis by administration of MR16-1 or control Ab to either PBS- or BLM-treated mice (n = 3~4 for each group). The effect of Ab therapy was assessed on day 56. **B:** H&E staining of specimens derived from PBS- or BLM-injected mice treated with MR16-1 or control Ab (original magnification, ×40), and measurements of dermal thickness (**C**) (the measurement region of dermal thickness was indicated with the length of each **two-headed arrow** in **B**) and skin hardness (**D**). The number of α-SMA–positive fibroblasts (**E**) and mast cells (**F**) per HPF (×400) were determined by observation of 10 random grids. The value graphed is the average of the observation of 10 grids for each of the four mice in the group. **C** to **F:** Bars represent mean ± SD. $^*P < 0.05$. $^{**}P < 0.01$, one-way analysis of variance and Bonferroni post hoc multiple comparison. Data presented are from the first of two independent experiments with similar results. See Table 2 for data from both experiments.

IL-6 Directly Modulates α-SMA Expression in Dermal Fibroblasts in Vitro

We next focused on whether dermal fibroblasts are a target of IL-6. Nontreated primary dermal fibroblasts from wild-type mice already express α-SMA, and stimulation with exogenous recombinant mouse IL-6 (rmIL-6) did not alter α-SMA expression (Figure 4A). Further, highly expressed levels of endogenous IL-6 from nontreated cultured primary wild-type dermal fibroblasts and decreased levels of α-SMA mRNA expression after MR16 treatment indicated that hyporesponsiveness of cultured primary wild-type dermal fibroblasts to exogenous IL-6 was presumably due to the autocrine regulation of α-SMA by IL-6 (Figure 4B). Thus, we switched to primary *Il*-6KO mouse–derived fibroblasts and evaluated α-SMA expression using immunofluorescent staining and Western blot analysis. Low-level expression was observed in nontreated *Il*-6KO dermal fibroblasts, but stimulation with 1 or 10 ng/mL of rmIL-6 induced α-SMA expression in a dose-dependent manner (Figure 4A). α-SMA induction by rmIL-6 was inhibited by 10 ng/mL MR16-1 and also by the ERK1/2 inhibitor PD98059 (Figure 4C).

These results led us to examine whether the positive effects of clinical treatment with tocilizumab might correlate with reduced numbers of ERK-activated α-SMA–pos-

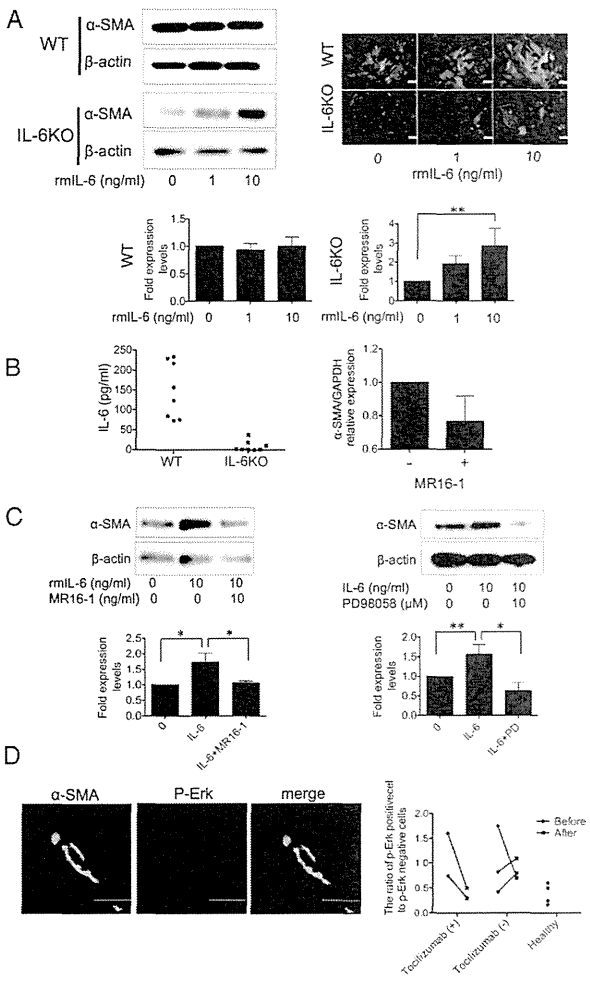

Figure 4. IL-6 induces α-SMA protein expression in cultured *Il*-6KO fibroblasts. **A:** α-SMA expression following recombinant mouse IL-6 (rmIL-6) stimulation was determined by immunofluorescent staining and Western blot analysis. α-SMA and nucleus were show in green and blue, respectively. Scale bar = 100 μm. β-Actin expression was used to determine fold changes in expression by densitometry. Cultured dermal fibroblasts from wild-type (WT) and *Il*-6KO mice were treated with 0, 1, and 10 ng/mL rmIL-6 for 24 hours. These experiments were repeated three times, and the results of densitometric analyses are presented as the fold change (mean ± SD) compared with control. $^{**}P < 0.01$, one-way analysis of variance and Bonferroni post hoc multiple comparisons. **B:** *Il*-6 levels in supernatants of cultured dermal fibroblasts from WT and *Il*-6KO mice (**left**) after 24 hours. MR16-1 treatment decreased α-SMA mRNA expression in cultured primary WT dermal fibroblasts (**right**). **C:** MR16-1 and ERK inhibitor, PD98058, attenuated rmIL-6–induced α-SMA protein expression in cultured *Il*-6KO fibroblasts. β-Actin expression was used to determine fold changes in expression by densitometry. These experiments were performed three times, and the results of densitometric analyses are presented as the fold change (mean ± SD) compared with control. $^{**}P < 0.01$, $^*P < 0.05$, one-way analysis of variance and Bonferroni post hoc multiple comparisons. **D:** Immunofluorescent staining for phosphorylated ERK (p-ERK, red) and α-SMA (green) in lesional skin derived from two tocilizumab-treated patients with scleroderma. A representative image of p-ERK$^+$, α-SMA$^+$ fibroblasts (original magnification, ×1,200) is shown. The number of p-ERK–positive α-SMA–positive fibroblasts per HPF (×400) was determined by observation of 10 random grids. Scale bar = 50 μm. The ratio of p-ERK–positive fibroblasts was calculated as follows: the number of p-ERK$^+$, α-SMA$^+$ fibroblasts/the number of p-ERK$^-$, α-SMA$^+$ fibroblasts.

itive dermal fibroblasts in lesional skin of scleroderma patients. The number of Erk-activated α-SMA–positive cells in lesional skin in scleroderma patients treated with tocilizumab for 6 months was reduced to a similar level as in healthy skin, whereas the number in scleroderma patients treated with 10 mg/day of prednisolone for 6 months without tocilizumab was diminished in one patient and increased in two patients (Figure 4D).

Attenuated BLM-Induces Dermal Sclerosis in Il-6KO Mice

To investigate the role of IL-6 in BLM-induced dermal sclerosis, *Il-6*KO mice received subcutaneous injection of BLM or PBS for 4 weeks, and histological and physical examination of the lesional skin was performed (Figure 5A, Table 3). We found that BLM-induced dermal sclerosis in *Il-6*KO mice was attenuated compared with that in wild-type mice. Lack of visible changes in the skin between PBS-treated *Il-6*KO mice and PBS-treated wild-type mice indicated that IL-6 might not be involved in dermal homeostasis (Figure 5A). After 4 weeks of BLM treatment, dermal thickness and skin hardness in *Il-6*KO mice were significantly attenuated compared to wild-type mice (Figure 5A). The numbers of α-SMA–positive cells and mast cells in BLM-treated *Il-6*KO mice were significantly reduced compared to BLM-treated wild-type mice (Figure 5B). Table 3 summarizes the data from two experiments. These results indicate that IL-6 is likely to play an important role in promoting the fibrogenic responses elicited by BLM treatment.

Enlarged Draining LNs Are Reduced in Size by a Block of IL-6 in the Mouse Model and in a Patient with Scleroderma

We found that cutaneous draining LNs were visibly enlarged by BLM treatment in the scleroderma model mice, but not by PBS treatment (Figure 6A, Table 4). The total LN cell count per LN in control Ab–treated BLM-injected mice was significantly increased compared with control Ab–treated PBS-injected mice, and decreased by administration of MR16-1 to BLM-injected mice. Although it was only from a single experiment with a small number of mice, the weight per LN also showed similar findings to the results of the total LN cell count per LN. However, no histological differences were observed between LNs from BLM- and PBS-injected control Ab–treated mice (Figure 6A). Detailed cell fractionation analysis (using cell-surface antigens CD4, CD8, B220, CD11c, F4/80, and PDCA1) of cells isolated from the draining LNs revealed that the ratio of $PDCA1^+CD11c^+$ double-positive cells [plasmacytoid dendritic cells (pDCs)] was significantly increased in the draining LNs of prophylactically MR16-1–treated model mice (Figure 6B). Further, draining LNs were not grossly enlarged in BLM-treated *Il-6*KO mice (Figure 6C, Table 4), consistent with weight and total cell count per LN measurements in the normal range (Figure 6C).

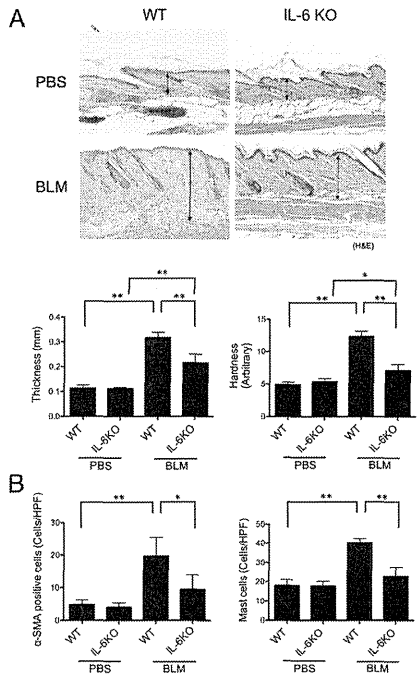

Figure 5. Attenuated BLM-induced dermal sclerosis in *Il-6*KO mice. **A:** H&E staining of skin specimen derived from PBS- and BLM-treated wild-type (WT) and *Il-6*KO mice (original magnification × 40), and measurements of dermal thickness (**lower left panel**) and skin hardness (**lower right panel**). The length of the **two-headed arrows** indicates the measurement region of dermal thickness. **B:** The number of α-SMA–positive fibroblasts (**left panel**) and mast cells (**right panel**) per HPF (×400) was determined by observation of 10 random grids. **A** and **B:** Bars represent mean ± SD ($n = 4$ for each group). $^*P < 0.05$, $^{**}P < 0.01$, one-way analysis of variance and Bonferroni post hoc multiple comparison. Data presented are from the first of two independent experiments that yielded similar results, and Table 3 presents data from both experiments.

We then examined whether LNs were enlarged in a patient with scleroderma, and found swelling of axillary LNs on computed tomography scan (Figure 6D), which was not detected after the administration of tocilizumab (Figure 6D).

Discussion

Our study demonstrates the critical role of IL-6 in dermal sclerosis. Blockade of IL-6 receptor with MR16-1 in the BLM-treated mice alleviates dermal sclerosis. This report also addresses outstanding problems in scleroderma pathogenesis, including the target of IL-6.

The source(s) of the elevated IL-6 in the sera of patients with scleroderma are still unclear. Several lines of

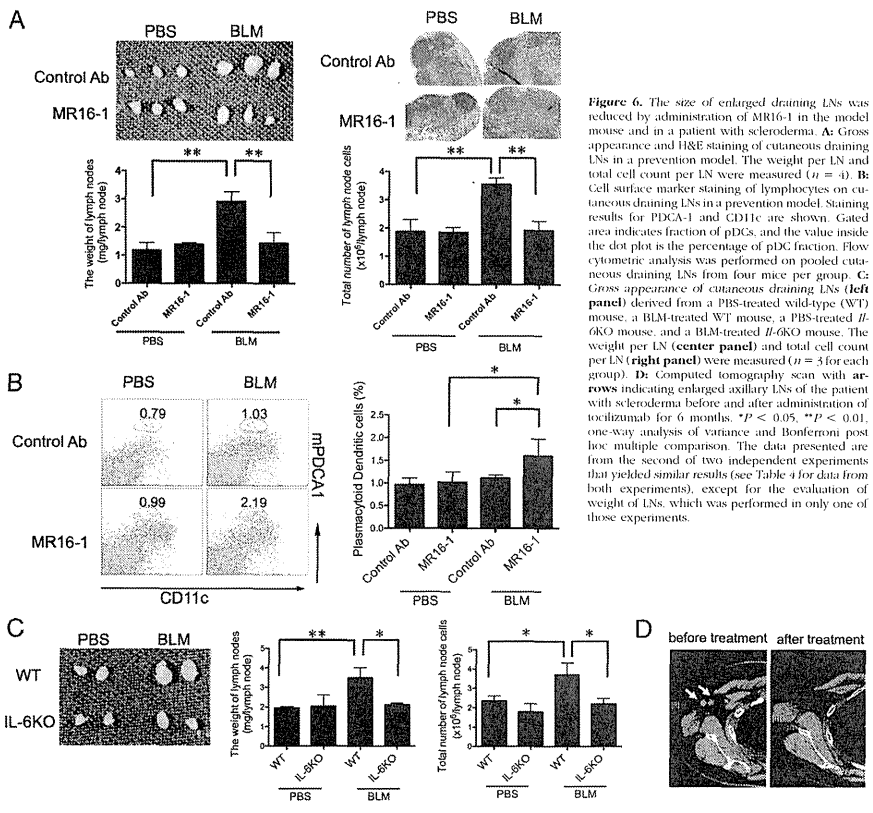

Figure 6. The size of enlarged draining LNs was reduced by administration of MR16-1 in the model mouse and in a patient with scleroderma. **A:** Gross appearance and H&E staining of cutaneous draining LNs in a prevention model. The weight per LN and total cell count per LN were measured ($n = 4$). **B:** Cell surface marker staining of lymphocytes on cutaneous draining LNs in a prevention model. Staining results for PDCA-1 and CD11c are shown. Gated area indicates fraction of pDCs, and the value inside the dot plot is the percentage of pDC fraction. Flow cytometric analysis was performed on pooled cutaneous draining LNs from four mice per group. **C:** Gross appearance of cutaneous draining LNs (**left panel**) derived from a PBS-treated wild-type (WT) mouse, a BLM-treated WT mouse, a PBS-treated *Il-6*KO mouse, and a BLM-treated *Il-6*KO mouse. The weight per LN (**center panel**) and total cell count per LN (**right panel**) were measured ($n = 5$ for each group). **D:** Computed tomography scan with **arrows** indicating enlarged axillary LNs of the patient with scleroderma before and after administration of tocilizumab for 6 months. $^*P < 0.05$, $^{**}P < 0.01$, one-way analysis of variance and Bonferroni post hoc multiple comparison. The data presented are from the second of two independent experiments that yielded similar results (see Table 4 for data from both experiments), except for the evaluation of weight of LNs, which was performed in only one of those experiments.

evidence suggest peripheral blood mononuclear cells are a source. The supernatant concentration of IL-6 was reported to be statistically significantly elevated in peripheral blood mononuclear cells[6,20,21] and in T-cell lines[6] derived from patients with systemic sclerosis compared with healthy controls. It also has been reported that experimentally activated B cells might be prone to produce IL-6.[22,23] Other lines of evidence implicate dermal fibroblasts as an important source of IL-6.[13,24–28] In this report, although the expression of IL-6 mRNA in both lesional skin and draining LNs was increased by BLM treatment, the specific cell type producing IL-6 was not identified. Further studies are required to clarify the source(s) of IL-6.

How does secreted IL-6 contribute to the pathogenesis of scleroderma? IL-6 might modulate α-SMA expression in dermal fibroblasts and induce myofibroblasts, which are known to produce collagen[29] and induce sclerotic change.[11,30] We observed IL-6 effects on α-SMA expression from *Il-6*KO dermal fibroblasts *in vitro* in this study (Figure 4A). Unexpectedly, nontreated cultured wild-type dermal fibroblasts strongly expressed α-SMA (Figure 4A), the expression of which was not affected by exogenous IL-6, whereas MR16-1 treatment decreased the expression of α-SMA mRNA (Figure 4, A and B). Therefore, continuous autocrine production of IL-6 by wild-type cultured dermal fibroblasts might increase the threshold for reactivity to IL-6.

Furthermore, in both prevention and treatment protocols with MR16-1, the reduction in dermal sclerosis was accompanied by decreasing numbers of myofibroblasts, which are known as activated fibroblasts with strong fibrogenic property. The absence of myofibroblasts at the BLM injection site of *Il-6*KO mice indicates that IL-6–induced dermal sclerosis occurs via induction of myofibroblasts. Thus, we hypothesize that MR16-1 and tocilizumab have favorable effects on scleroderma via prevention of fibroblast activation. Administration of tocili-

zumab to scleroderma patients exhibited ameliorating effects of skin sclerosis,[15] and seemed to reduce the number of Erk-activated α-SMA–positive fibroblast in lesional skin (Figure 4D). These findings were inconclusive because of the number of cases, and further studies were required.

Another finding was reduction of LN swelling by MR16-1 treatment in mice in the BLM-induced model of scleroderma. We could not determine whether the LN swelling associated with BLM treatment was a cause or effect of BLM-induced skin sclerosis. Examination of the differential ratios of leukocytes, such as T cells, B cells, and macrophages, did not give any insight, as these were not altered after 4 weeks of BLM injection (data not shown). However, there was a slight, but significant, increase in the numbers of cells double-positive for PDCA-1^+CD11c^+ (Figure 6D) or $B220^+CD11c^+$ (data not shown) in the draining LNs of MR16-1–treated mice relative to control Ab–treated mice in the prevention model. This suggests that IL-6 might affect pDC numbers in the LNs. LN swelling is not a well-known symptom in scleroderma, and only a few articles describe LN findings in scleroderma.[31] We should keep an eye on such symptoms.

Recent studies have indicated that pDCs may promote scleroderma via secretion of type 1 interferon,[32] and induction of type 1 interferon was found by anti-topoisomerase antibody-containing serum, but not by anti-centromere antibody.[32,33] However, other data suggest MHC class II–restricted antigen presentation by pDCs might inhibit T-cell–mediated autoimmunity via selective expansion of Ag-specific natural regulatory T cells.[34] Because MHC class II–restricted proliferation of $CD4^+$ T cells had been previously thought to contribute to the pathogenesis of scleroderma,[35] one could speculate that an increased ratio of pDCs might prevent skin sclerosis via regulating peripheral tolerance. However, it is clear that the function of pDCs in pathogenesis of scleroderma is complex and needs further study.

The clear positive effects of IL-6 inhibition in mouse models with scleroderma indicate that further study of IL-6–secreting cells, effectors, and signaling in scleroderma holds great promise for the development of therapies for scleroderma, as well as for other diseases in which IL-6 can play a pivotal role.

Acknowledgments

We thank Prof. Junji Takeda (Osaka University) for expert comments and Dr. Toshiaki Hanafusa, Kenjyu Nishida, and Han Fu for technical assistance.

References

1. Preliminary criteria for the classification of systemic sclerosis (scleroderma). Subcommittee for scleroderma criteria of the American Rheumatism Association Diagnostic and Therapeutic Criteria Committee. Arthritis Rheum 1980, 23:581–590
2. Needleman BW, Wigley FM, Stair RW: Interleukin-1, interleukin-2, interleukin-4, interleukin-6, tumor necrosis factor alpha, and interferon-gamma levels in sera from patients with scleroderma. Arthritis Rheum 1992, 35:67–72
3. Hebbar M, Gillot JM, Hachulla E, Lassalle P, Hatron PY, Devulder B, Janin A: Early expression of E-selectin, tumor necrosis factor alpha, and mast cell infiltration in the salivary glands of patients with systemic sclerosis. Arthritis Rheum 1996, 39:1161–1165
4. Terao M, Murota H, Kitaba S, Katayama I: Tumor necrosis factor-alpha processing inhibitor-1 inhibits skin fibrosis in a bleomycin-induced murine model of scleroderma. Exp Dermatol 2009, 19:38–43
5. Murota H, Hamasaki Y, Nakashima T, Yamamoto K, Katayama I, Matsuyama T: Disruption of tumor necrosis factor receptor p55 impairs collagen turnover in experimentally induced sclerodermic skin fibroblasts. Arthritis Rheum 2003, 48:1117–1125
6. Scala E, Pallotta S, Frezzolini A, Abeni D, Barbieri C, Sampogna F, De Pita O, Puddu P, Paganelli R, Russo G: Cytokine and chemokine levels in systemic sclerosis: relationship with cutaneous and internal organ involvement. Clin Exp Immunol 2004, 138:540–546
7. Yamamoto T, Takagawa S, Katayama I, Yamazaki K, Hamazaki Y, Shinkai H, Nishioka K: Animal model of sclerotic skin. I: local injections of bleomycin induce sclerotic skin mimicking scleroderma. J Invest Dermatol 1999, 112:456–462
8. Yamamoto T, Takagawa S, Katayama I, Nishioka K: Anti-sclerotic effect of transforming growth factor-beta antibody in a mouse model of bleomycin-induced scleroderma. Clin Immunol 1999, 92:6–13
9. Kuwana M, Medsger TA Jr., Wright TM: Analysis of soluble and cell surface factors regulating anti-DNA topoisomerase I autoantibody production demonstrates synergy between Th1 and Th2 autoreactive T cells. J Immunol 2000, 164:6138–6146
10. Kishimoto T: The biology of interleukin-6. Blood 1989, 74:1–10
11. Gallucci RM, Lee EG, Tomasek JJ: IL-6 modulates alpha-smooth muscle actin expression in dermal fibroblasts from IL-6-deficient mice. J Invest Dermatol 2006, 126:561–568
12. Duncan MR, Berman B: Stimulation of collagen and glycosaminoglycan production in cultured human adult dermal fibroblasts by recombinant human interleukin 6. J Invest Dermatol 1991, 97:686–692
13. Kawaguchi Y, Hara M, Wright TM: Endogenous IL-1alpha from systemic sclerosis fibroblasts induces IL-6 and PDGF-A. J Clin Invest 1999, 103:1253–1260
14. Nishimoto N, Kishimoto T: Interleukin 6: from bench to bedside. Nat Clin Pract Rheumatol 2006, 2:619–626
15. Shima Y, Kuwahara Y, Murota H, Kawai M, Hirano T, Arimitsu J, Narazaki M, Hagihara K, Ogata A, Katayama I, Kawase I, Kishimoto T, Tanaka T: The skin of patients with systemic sclerosis softened during the treatment with anti-IL-6 receptor antibody tocilizumab. Rheumatology 2010, 49:2408–12
16. Gallucci RM, Sloan DK, Heck JM, Murray AR, O'Dell SJ: Interleukin 6 indirectly induces keratinocyte migration. J Invest Dermatol 2004, 122:764–772
17. Kopf M, Baumann H, Freer G, Freudenberg M, Lamers M, Kishimoto T, Zinkernagel R, Bluethmann H, Kohler G: Impaired immune and acute-phase responses in interleukin-6-deficient mice. Nature 1994, 368:339–342
18. Takagi N, Mihara M, Moriya Y, Nishimoto N, Yoshizaki K, Kishimoto T, Takeda Y, Ohsugi Y: Blockage of interleukin-6 receptor ameliorates joint disease in murine collagen-induced arthritis. Arthritis Rheum 1998, 41:2117–2121
19. Kuwahara Y, Shima Y, Shirayama D, Kawai M, Hagihara K, Hirano T, Arimitsu J, Ogata A, Tanaka T, Kawase I: Quantification of hardness, elasticity and viscosity of the skin of patients with systemic sclerosis using a novel sensing device (Vesmeter): a proposal for a new outcome measurement procedure. Rheumatology (Oxford) 2008, 47:1018–1024
20. Hasegawa M, Sato S, Ihn H, Takehara K: Enhanced production of interleukin-6 (IL-6), oncostatin M and soluble IL-6 receptor by cultured peripheral blood mononuclear cells from patients with systemic sclerosis. Rheumatology (Oxford) 1999, 38:612–617
21. Crestani B, Seta N, De Bandt M, Soler P, Rolland C, Dehoux M, Boutten A, Dombret MC, Palazzo E, Kahn MF, et al.: Interleukin 6 secretion by monocytes and alveolar macrophages in systemic sclerosis with lung involvement. Am J Respir Crit Care Med 1994, 149:1260–1265
22. Saito E, Fujimoto M, Hasegawa M, Komura K, Hamaguchi Y, Kaburagi Y, Nagaoka T, Takehara K, Tedder TF, Sato S: CD19-dependent B lymphocyte signaling thresholds influence skin fibrosis and autoimmunity in the tight-skin mouse. J Clin Invest 2002, 109:1453–1462
23. Matsushita T, Hasegawa M, Yanaba K, Kodera M, Takehara K, Sato S: Elevated serum BAFF levels in patients with systemic sclerosis: enhanced BAFF signaling in systemic sclerosis B lymphocytes. Arthritis Rheum 2006, 54:192–201
24. Takemura H, Suzuki H, Fujisawa H, Yuhara T, Akama T, Yamane K, Kashiwagi H: Enhanced interleukin 6 production by cultured fibroblasts from patients with systemic sclerosis in response to platelet derived growth factor. J Rheumatol 1998, 25:1534–1539
25. Kawaguchi Y, Nishimagi E, Tochimoto A, Kawamoto M, Katsumata Y, Soejima M, Kanno T, Kamatani N, Hara M: Intracellular IL-1alpha-binding proteins contribute to biological functions of endogenous IL-1alpha in systemic sclerosis fibroblasts. Proc Natl Acad Sci U S A 2006, 103:14501–14506
26. Fukasawa C, Kawaguchi Y, Harigai M, Sugiura T, Takagi K, Kawamoto M, Hara M, Kamatani N: Increased CD40 expression in skin fibroblasts from patients with systemic sclerosis (SSc): role of CD40-CD154 in the phenotype of SSc fibroblasts. Eur J Immunol 2003, 33:2792–2800
27. Kadono T, Kikuchi K, Ihn H, Takehara K, Tamaki K: Increased production of interleukin 6 and interleukin 8 in scleroderma fibroblasts. J Rheumatol 1998, 25:296–301
28. Koch AE, Kronfeld-Harrington LB, Szekanecz Z, Cho MM, Haines GK, Harlow LA, Strieter RM, Kunkel SL, Massa MC, Barr WG, Jimenez SA: In situ expression of cytokines and cellular adhesion molecules in the skin of patients with systemic sclerosis. Their role in early and late disease. Pathobiology 1993, 61:239–246
29. Wynn TA: Cellular and molecular mechanisms of fibrosis. J Pathol 2008, 214:199–210
30. Kirk TZ, Mark ME, Chua CC, Chua BH, Mayes MD: Myofibroblasts from scleroderma skin synthesize elevated levels of collagen and tissue inhibitor of metalloproteinase (TIMP-1) with two forms of TIMP-1. J Biol Chem 1995, 270:3423–3428
31. Ofstad E: Scleroderma (progressive systemic sclerosis). A case involving polyneuritis and swelling of the lymph nodes. Acta Rheumatol Scand 1960, 6:65–75
32. Eloranta ML, Franck-Larsson K, Lovgren T, Kalamajski S, Ronnblom A, Rubin K, Alm GV, Ronnblom L: Type I interferon system activation and association with disease manifestations in systemic sclerosis. Ann Rheum Dis 2010, 69:1396–1402
33. Kim D, Peck A, Santer D, Patole P, Schwartz SM, Molitor JA, Arnett FC, Elkon KB: Induction of interferon-alpha by scleroderma sera containing autoantibodies to topoisomerase I: association of higher interferon-alpha activity with lung fibrosis. Arthritis Rheum 2008, 58:2163–2173
34. Irla M, Kupfer N, Suter T, Lissilaa R, Benkhoucha M, Skupsky J, Lalive PH, Fontana A, Reith W, Hugues S: MHC class II-restricted antigen presentation by plasmacytoid dendritic cells inhibits T cell-mediated autoimmunity. J Exp Med 2010, 207:1891–1905
35. Kuwana M, Medsger TA Jr., Wright TM: T cell proliferative response induced by DNA topoisomerase I in patients with systemic sclerosis and healthy donors. J Clin Invest 1995, 96:586–596

Pigment Cell Melanoma Res. 25; 219–230

ORIGINAL ARTICLE

Dysregulation of melanocyte function by Th17-related cytokines: significance of Th17 cell infiltration in autoimmune vitiligo vulgaris

Yorihisa Kotobuki[1,2,*], Atsushi Tanemura[1,*], Lingli Yang[1,2], Saori Itoi[1], Mari Wataya-Kaneda[1], Hiroyuki Murota[1], Minoru Fujimoto[2], Satoshi Serada[2], Tetsuji Naka[2] and Ichiro Katayama[1]

1 Department of Dermatology Integrated Medicine, Osaka University Graduate School of Medicine, Osaka, Japan 2 Laboratory for Immune Signal, National Institute of Biomedical Innovation

CORRESPONDENCE Atsushi Tanemura, e-mail: tanemura@derma.med.osaka-u.ac.jp
*These authors contributed equally to this work.

KEYWORDS vitiligo/Th17 cell/Th17-related cytokines/melanocyte/interaction with skin-resident cells

PUBLICATION DATA Received 19 July 2011, revised and accepted for publication 30 November 2011, published online 3 December 2011

doi: 10.1111/j.1755-148X.2011.00945.x

Summary

The aim of this study was to determine whether CD4$^+$IL-17A$^+$Th17 cells infiltrate vitiligo skin and to investigate whether the proinflammatory cytokines related to Th17 cell influence melanocyte enzymatic activity and cell fate. An immunohistochemical analysis showed Th17 cell infiltration in 21 of 23 vitiligo skin samples in addition to CD8$^+$ cells on the reticular dermis. An in vitro analysis showed that the expression of MITF and downstream genes was downregulated in melanocytes by treatment with interleukin (IL)-17A, IL-1β, IL-6, and tumor necrosis factor (TNF)-α. Treatment with these cytokines also induced morphological shrinking in melanocytes, resulting in decreased melanin production. In terms of local cytokine network in the skin, IL-17A dramatically induced IL-1β, IL-6, and TNF-α production in skin-resident cells such as keratinocytes and fibroblasts. Our results provide evidence of the influence of a complex Th17 cell-related cytokine environment in local depigmentation in addition to CD8$^+$ cell-mediated melanocyte destruction in autoimmune vitiligo.

Introduction

In the epidermis, the epidermal melanin unit is reliant on the close interaction between a melanocyte and the associated pool of keratinocytes, and several inflammatory cytokines affect melanocyte migration, proliferation, and differentiation. Therefore, the local skin microenvironment generated by the skin-resident cells may be considered a crucial milieu for the normal life and functions of epidermal melanocytes (Chalraborty and Pawelek, 1993).

Vitiligo, a representative depigmented skin disorder associated with melanocyte destruction, affects an estimated 1% of the world's population (Howitz et al., 1977). Although the cellular immunoresponse, mainly of CD8$^+$ cytotoxic T cells, to the melanocyte-specific proteins MART-1, tyrosinase (TYR), and TRPs-1 and -2 has been shown to destroy functional melanocytes in autoimmune vitiligo, this does not provide a full explanation for the etiology of vitiligo (Norris et al., 1994; Ogg et al., 1998; Okamoto et al., 1998; Ongenae et al., 2003). In addition to the autoimmune mechanism, recent reports have shown that there is a significant increase in the expression of inflammatory cytokines in affected skin compared with unaffected skin, and several investigators have proposed that the influence of local cytokines may be related to the induction and maintenance of vitiligo (Basak et al., 2009; Moretti et al., 2002, 2009; Ratsep et al., 2008). Although the representative cytokines increased in vitiligo skin have been reported to include interleukin (IL)-2, tumor necrosis factor (TNF)-α, and interferon (IFN)-γ (Caixia et al., 1999), there is no direct evidence of their function in the melanocyte destruction observed in vitiligo.

Upon induction by transforming growth factor (TGF)-b and IL-6, a subset of CD4$^+$ helper T cells develops as Th17 cells (Diveu et al., 2008). IL-17A is a cystine-linked homodimeric proinflammatory cytokine produced by Th17 cells, which form a distinct subset of the CD4$^+$ T-cell lineage. IL-17A stimulates the production of IL-1β, TNF-α, and IL-6 (Kolls and Linden, 2004; Liang et al., 2006). In the past decade, Th17 cells have been identified in autoimmune skin inflammatory disorders such as psoriasis and atopic dermatitis (Asarch et al., 2008; Fitch et al., 2009). A recent study showed a positive correlation between serum IL-17 levels and the extent of the depigmentation patch area in vitiligo, thus suggesting that Th17 cells, rather than regulatory T cells, are involved in vitiligo (Basak et al., 2009). Another study demonstrated elevated IL-17 levels in lesional skin and serum of patients with vitiligo compared with those of controls (Bassiouny and Shaker, 2011). These results indicated the importance of the secreted cytokine environment surrounding vitiliginous melanocytes in terms of vitligo etiology. In the present study, we investigated whether Th17 cells infiltrate vitiligo skin as in cases of psoriasis and whether the proinflammatory cytokines produced by Th17 cells, keratinocytes, and fibroblasts are altered in vitiligous lesions in a series of non-segmental vitiligo patients. The Th17-related cytokines tested included IL-17A and IL-22, in addition to IL-1β and IL-6, which have been reported to inhibit melanocyte activity (Kamaraju et al., 2002; Kholmanskikh et al., 2010).

MITF-M (microphthalmia-associated transcription factor-M) is a master transcription factor regulating melanocyte fate and melanogenic activity; it is distinctly expressed in melanocytes and mast cells (Levy et al., 2006). MITF expression and phosphorylation are important for the regulation of melanogenesis and melanocyte survival because the target genes of MITF encode the apoptosis regulator protein, B-cell lymphoma 2 (Bcl-2), in addition to melanogenic enzymes, tyrosinase, tyrosinase-related protein-1 (TRP-1), and dopachrome tautomerase (DCT), which are indispensable for maintaining melanocyte function (Levy et al., 2006). Because of the reduction in active melanocytes expressing these proteins in the vitiligo epidermis, the dysregulation of MITF expression has to be resolved to effectively treat vitiligo. In addition, the mRNA levels of *MITF* and *BCL2* were decreased in the lesional skin compared with the non-lesional skin of vitiligo patients (Kingo et al., 2008). The expression levels of IL-6 and TNF-α were also significantly higher in the lesional skin, indicating that in vitiligo lesions, there is increased expression of cytokines that are paracrine inhibitors of melanocytes (Moretti et al., 2002, 2009). These cytokines are produced mainly by keratinocytes, so it is possible that these cells may be abnormal in vitiligo. In addition, the expression of cytokines was unchanged in healthy skin compared with non-lesional skin, suggesting that the change observed in vitiligo lesional skin is possibly related to, or contributes to, depigmentation. Therefore, it is conceivable that there is a previously unrecognized mechanism involved in the regulation of the pigmentation-hypopigmentation balance in addition to a cytotoxic effect by CD8$^+$ T cell.

In this study, we examined the direct effect of Th17-related cytokines on MITF expression to determine the effects on the resulting cytokine involvement on the regulation of critical melanocyte behavior. We discuss the significance of Th17 cell infiltration in autoimmune vitiligo skin and propose a functional involvement of Th17 cell-related proinflammatory cytokines in vitiligo.

Significance

Here we show that not only cytotoxic T cells, which have been thought to play a major role in autoimmune vitiligo, but also infiltration of Th17 cells may play a role in vitiligo skin. In fact, we find that in vitro, a network of Th17 cell-related cytokines directly affect melanocyte activity and function, including downregulation of melanin production and shrinkage of melanocytes. These observations may shed light on the functional significance of TH17 cells in autoimmune vitiligo.

Results

Vitiligo skin develops in association with Th17 cell infiltration

Approval for this study was obtained from the Institutional Review Board of the Osaka University Hospital. To investigate whether Th17 cells infiltrate vitiligo skin, we performed immunostaining for IL-17A and CD4 using specific antibodies. Th17 cells were defined as the cells expressing both markers after exclusion of gamma delta T cells. Twenty-three vitiligo patients were enrolled in this study (see Table 1 for details) and were divided into 17 generalized, four localized, and two seg-

Table 1. Patients' characteristics and the infiltration status of Th17 cells

Age	27–81			
Gender				
Female	13			
Male	10			
Disease duration (yr)	0.1–26			
Mean	6.2			
	(n)	>50/field	<50/field	Not detected
Th17 cell infiltration				
Generalized type	17	11	6	0
Segmental type	4	2	0	2
Localized type	2	2	0	0
Total	23	15	6	2

mental types. The ages of the enrolled patients ranged from 27 to 81 yr, and the subjects included 13 women and 10 men. As a representative case, we show a 79-yr-old man who had experienced enlarging symmetrical depigmented macules on the whole body including face starting 2 yr previously who was positive for antithyroid antibody in the blood test (Figure 1).

Biopsy specimens were obtained from the leading edge of lesional skin on the left upper arm and were processed for the designated immunostaining. The immunohistochemical analysis revealed significant infiltration of IL-17A$^+$CD4$^+$ cells, that is, Th17 cells, mainly on the reticular dermis and perivascular region (Figure 1A). IL-17A expression was confirmed by RT-PCR using vitiligo tissue RNA. Psoriasis skin, a representative skin disease with Th17 cell infiltration, was loaded as a positive control for RT-PCR (Figure 1A). CD8$^+$ T cells were also observed, mainly below the epidermis, whereas Foxp3$^+$ cells and CD20$^+$ B cells had only faintly infiltrated (Figure 1B). Melan-A positive melanocytes were not observed in the vitiligo epidermis with inflammatory cell infiltration, whereas they were frequently located in the non-lesional skin (Figure 1B lower right panel and Inbox, respectively).

We observed a significant number of Th17 cells in 21 of 23 of the patient skin samples, and more than 50 double-positive cells per high power field were observed in 15 patients, while there was sparse infiltration in normal skin. Th17 cells were not detected in the two cases of localized type. Psoriatic skin was used as a positive control for this staining and showed the involvement as dense infiltration through the epidermis and upper dermis of pathogenic inflammatory cells whose localization was different from that in vitiligo (Figure 1C). Although we suspected that early onset and generalized type vitiligo had more opportunity to be infiltrated by Th17 cells, there was no significant correlation between the number of infiltrating Th17 cells and the clinical type, or with disease parameters such as disease duration, age, or gender in 21 patients with Th17 cell infiltration (Figure 1E).

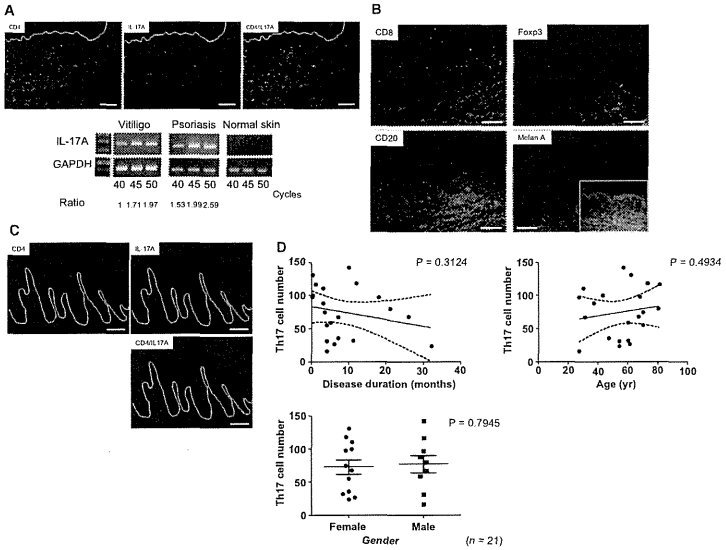

Figure 1. Photographic features of a representative generalized vitiligo patient and the immunohistochemical analysis for infiltrating cells in vitiligo skin. Multiple- and symmetrical-depigmented macules were present on the face and upper arm. A spindle-shaped skin specimen was obtained from the leading edge of an upper arm lesion. Immunostaining for CD4 and IL-17A in the vitiligo skin lesion indicated the significant infiltration of Th17 cells (yellow) positive for both CD4 (green) and IL-17A (red) mainly on reticular dermis and perivascular region. RT-PCR confirmed the same level of IL-17A expression in the vitiligo skin as in psoriasis skin (A). CD8-positive cytotoxic T lymphocytes (CTLs) (red, upper left) infiltrated the upper dermis and epidermis, whereas Foxp3 and CD20 positive cells (upper right and lower left) were only faintly detected. Melan-A-positive cells, highly differentiated melanocytes, were present in the normal region (lower right, small window), whereas they were absent in the vitiligo epidermis (lower right) (B). Psoriatic skin showed Th17 cell infiltration in the papillary dermis in addition to the epidermis (C). All images are original magnification ×40 for vitiligo and ×100 for psoriatic skin. The white bar indicates 100 μm. (D) The mean Th17 cell number present in vitiligo skin was counted on three independent fields, and the correlation with disease parameters such as disease duration, age, and gender was evaluated (n = 16).

Proinflammatory cytokines associated with Th17 cells influence in melanin activity

Because a significant number of Th17 cells were found in most of the vitiligo skin samples examined in this study, we hypothesized that there was a possible role for Th17 cell-related cytokines in melanocyte activity. Previous reports have shown that several cytokines downregulated tyrosinase activity through the activation of designated intracellular signaling pathways (Englaro et al., 1999; Kamaraju et al., 2002; Kholmanskikh et al., 2010). We therefore decided to examine the effects of IL-1β, IL-6, IL-17A, and IL-22, which are important cytokines induced by Th17 cell differentiation and maintenance, on melanocyte development and activity. MITF, a pivotal transcription factor related to melanocyte function and survival, expression and translocation was at first examined by immunocytochemistry (Figure 2A, C). Whereas there was apparent translocation of the MITF protein to the nucleus in untreated cultured melanocytes (Figure 2A), the MITF expression was decreased in the nucleus of the melanocytes treated with 10 ng/ml of IL-1β or IL-17A (Figure 2B, C), suggesting that there was a reduction in MITF-related signaling in melanocytes following cytokine treatment. In contrast, IL-22 treatment had no effect on melanocytes (data not shown), so we decided not to include IL-22 in the further experiments.

Next, we examined the expression of cytokine receptors by RT-PCR to confirm the ligand-to-receptor correspondence in melanocytes. Cultured human melanocytes were found to express IL-1R1, IL-6R, and IL-17RA without the addition of cytokines, whereas treatment with 10 ng/ml of their corresponding

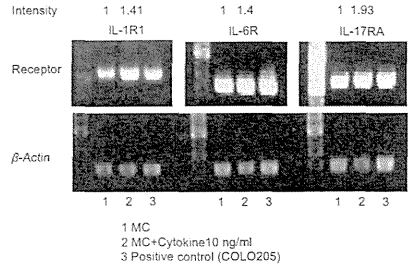

Figure 3. The expression of cytokine receptors in human melanocytes. IL-1R1, IL-6R, and IL-17RA mRNA were expressed in human melanocytes and were upregulated following treatment with their corresponding cytokines. COLO205 cells (colon cancer cell line) were used as a positive control. β-actin was used as a housekeeping gene.

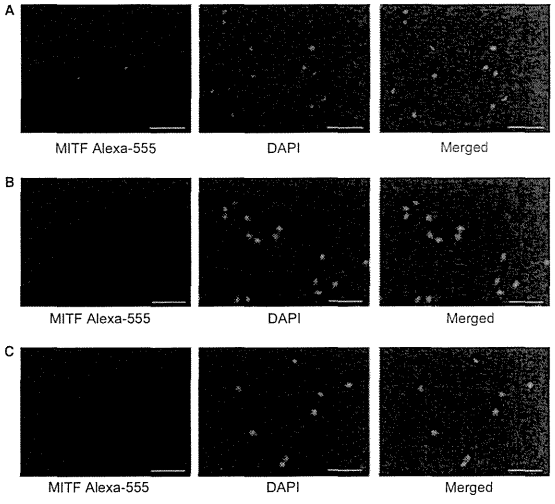

Figure 2. Immunocytochemical staining for MITF in human melanocytes. MITF was expressed mainly in the nuclei of untreated cells (A). In contrast, MITF expression was decreased after treatment with recombinant IL-1β (B) and IL-17A (C). The white bar indicates 50 μm.

cytokines increased receptor expression (Figure 3). COLO205 cells, the human colon cancer cell line expressing these receptors endogenously, were loaded in parallel with cultured melanocytes as a positive control.

To investigate the direct effects of Th17 cell-related cytokines on melanocytes in vitro, we examined the mRNA expression of melanogenic and melanocyte survival molecules after treatment of human melanocytes with recombinant human cytokines (Figure 4). The expression of *MITF*, which encodes a master transcription factor that regulates melanocyte function; of *TYR*, *TRP-1*, and *DCT*, which encode enzymes involved in melanin synthesis; and of *BCL2*, which encodes an anti-apoptotic protein, was measured by quantitative PCR. MITF expression was found to be significantly decreased in a dose-dependent manner after treatment with IL-1β, IL-6, and TNF-α (Figure 4A). The *MITF* transcription level decreased to <50% after treatment with 1 ng/ml of TNF-α. MITF was downregulated by 10 ng/ml IL-17A. In terms of the expression of its downstream enzymes, IL-1β significantly downregulated the genes, but only at a concentration of 10 ng/ml, whereas basic FGF upregulated their expression. IL-6 downregulated *TYRP1* and *DCT*, but there was no significant decrease in *TYR*. A 10 ng/ml concentration of IL-17A was needed to induce their significant downregulation. On the other hand, TNF-α significantly suppressed the expression of

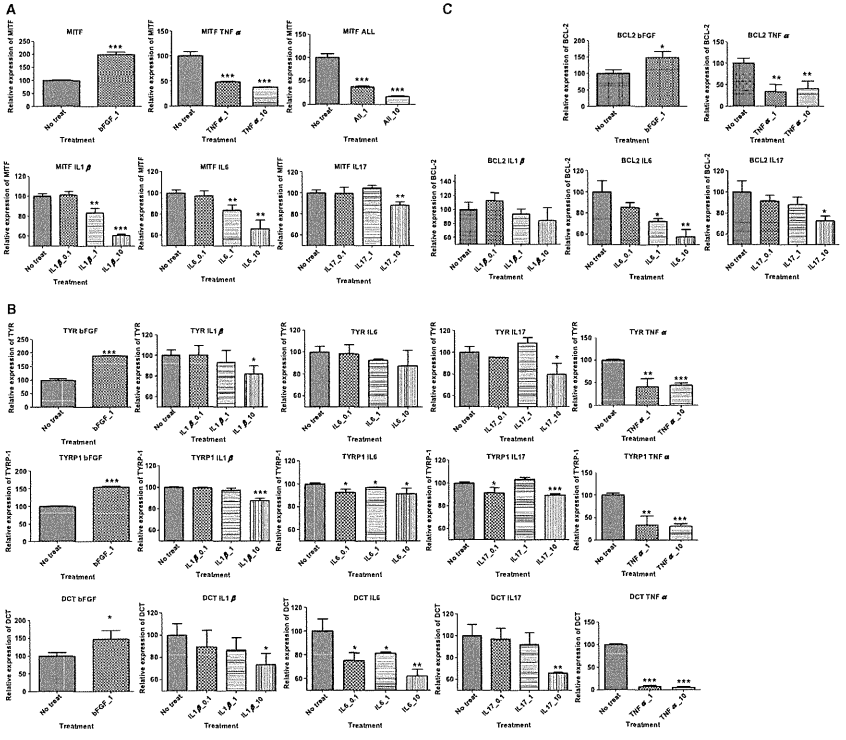

Figure 4. The quantitative analysis of the mRNA expression of MITF and genes encoding melanogenic enzymes. Human melanocytes were incubated with recombinant cytokines for 4 h at concentrations of 0.1, 1, or 10 ng/ml in the culture medium. The mRNA expression levels of MITF (A), genes encoding melanogenic enzymes (B), and B-cell lymphoma 2 (Bcl-2) (C) were measured by qRT-PCR. *P < 0.05; **P < 0.01; ***P < 0.001 compared with the expression level in untreated control cells.

these genes and *BCL2*, even at the concentration of 1 ng/ml, suggesting that TNF-α likely had the strongest suppressive effect on gene expression. BCL2 expression was decreased following treatment with IL-1β, IL-6, and IL-17A in a dose-dependent manner. Overall, there was a tendency for molecules related to melanocyte function to be downregulated following treatment with exogeneous cytokines (Figure 4B, C).

To determine the direct effects of Th17 cells on melanocytes, we performed coculture of the Th17 cells induced from peripheral blood mononuclear cells by an in vitro protocol with and without TGF-β treatment (Wilson et al., 2007) with melanocytes and real-time PCR. Th17-polarized cells without TGF-β decreased the expression of *MITF* and its downstream melanogenic molecules more than Th2-polarized cells did (Figure S1).

Furthermore, melanin production was measured after continuous treatment with exogenous cytokines including IL-1β, IL-6, IL-17A, and TNF-α. The percentage of melanin production was significantly lower in melanocytes treated with 1 and/or 10 ng/ml of exogenous cytokines than in untreated cells. In contrast, no reduction in total protein was observed after the addition of any of the cytokines (Figure 5). Because these cytokines are critical for the maintenance and development of Th17 cells from naïve CD4$^+$ T cells, we suggest that the presence of a specific local cytokine environment might be indispensable for Th17 cell recruitment and activation in vitiligo lesions, thereby indicating that they contribute significantly to depigmentation in addition to CTL (cytotoxic T cell) activation.

Production of cytokines by skin-resident cells

We have shown infiltration of Th17 cells in vitiligo skin and have demonstrated the inhibitory effects of Th17 cell-related cytokines on melanocyte function. As the cytokines examined in this study are produced not only by inflammatory cells but also by the surrounding cells, such as keratinocytes and fibroblasts, the source of the cytokine production was examined. We treated normal human epidermal keratinocyte (NHEK) and normal human dermal fibroblast (NHDF) cells with recombinant IL-17A and measured IL-1β, IL-6, and TNF-α production (Figure 6A, B). IL-17A exponentially increased the pro-

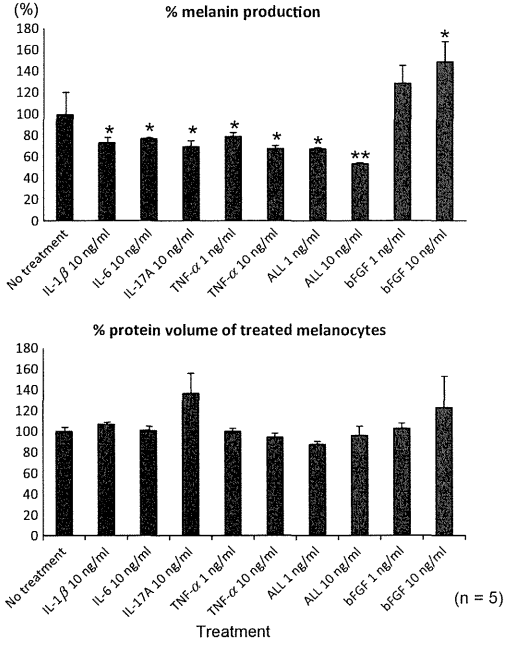

Figure 5. There is a decrease in melanin production after treatment with cytokines. Human melanocytes were incubated with 1 ng and/or 10 ng/ml of recombinant cytokines for 5 days in the culture medium (n = 5). Recombinant cytokines were added everyday. Cultured melanocytes were treated with 1 N NaOH and processed for absorbance at 450 nm to quantify the melanin volume. The protein volume of the cell extracts was measured to demonstrate whether the cytokines exerted the reduction of whole cell protein. *P < 0.05; **P < 0.01; ***P < 0.001 compared with the expression level of the untreated controls.

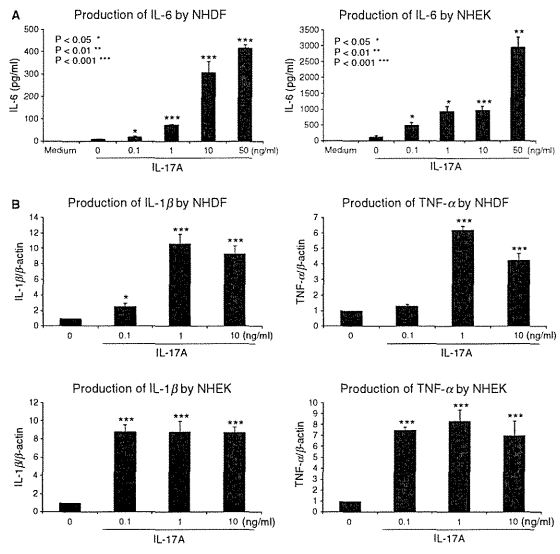

Figure 6. IL-17A induces the release of other Th17 cell-related cytokines from dermal fibroblasts and keratinocytes. (A) Human dermal fibroblasts and keratinocytes were incubated with recombinant IL-17A for 1 day at concentrations of 0.1, 1, 10, and 50 ng/ml in the culture medium, and the IL-6 secreted in the medium was measured by an ELISA. (B) After cells were incubated as in (A), the IL-1β and TNFα mRNA expression levels were measured by RT-PCR. *β-actin was used as a* housekeeping gene. *P < 0.05; **P < 0.01; ***P < 0.001 compared with the expression level of the untreated controls.

duction of these cytokines in a dose-dependent manner using both of these cell lines.

Cytokine-induced melanocyte dysfunction

Finally, we examined whether proinflammatory cytokines could directly induce melanocyte apoptosis and/or destruction in vitro. The cultured melanocytes were incubated with 1 and 10 ng/ml of recombinant IL-1β, IL-6, IL-17A, TNF-α, or all of the factors for 5 days, and then the melanocytes were observed microscopically under polarized light (Figure 7A). The cells were obviously aggregated and varied in shape after treatment with both the single cytokines and the cytokine cocktail, whereas the untreated cells and those treated with bFGF (basic fibroblast growth factor) grew with a spindle-shaped morphology. Staurosporine, a chemical that induces apoptosis by activating caspase-3, increased the number of round-shaped apoptotic melanocytes. TNF-α induced the greatest extent of melanocyte destruction compared with the other cytokines.

Next, melanocyte apoptosis was assessed by measuring caspase-3 activity after continuous treatment with 10 ng/ml of each of the individual cytokines and the cytokine cocktail. Staurosporine led to an increase in caspase-3 activity (Figure 7B), whereas there was no induction of caspase-3 activity following treatment with any of the cytokines. These results indicate that there *appears to be direct inhibition of melanocyte activity by* cytokines, rather than induction of cell apoptosis.

Discussion

In the present study, we identified a significant number of Th17 cells that had infiltrated vitiligo skin, and demonstrated *the inhibitory effect of Th17 cell-related proin*flammatory cytokines on melanocyte activity. We therefore hypothesize that the functional Th17 cell involvement in the initiation of psoriasis and atopic dermatitis may also play an important role in the pathogenesis of vitiligo. Although the precise pathogenic mechanisms underlying the induction of depigmentation in an immunological manner (Ongenae et al., 2003) still remain unknown, non-segmental vitiligo has been thought to be an autoimmune disease because of the high frequency of associated Hashimoto's thyroid disease (Daneshpazhooh et al., 2006; Hegedus et al., 1994; Schallreuter et al., 1994a), type I diabetes (Gould et al., 1985), collagen diseases with antinuclear antibodies (Mihailova et al., 1999), etc. Pathogenic antibodies were also detected in approximately 50% of vitiligo patients (Cui et al., 1992; Ruiz-Arguelles et al., 2007). With respect to the cellular immune condition, the infiltration of cytotoxic T cells targeting melanocyte-specific antigens in vitiligo lesions has been thought to play a critical role in hypopigmentation (Lang et al., 2001; Norris et al., 1994; Ogg et al., 1998). Recent reports have also suggested that there is the local environment *of proinflammatory cytokines such as* IL-1, IL-6, *and* TNF-α also contributes to the inhibition of melano-

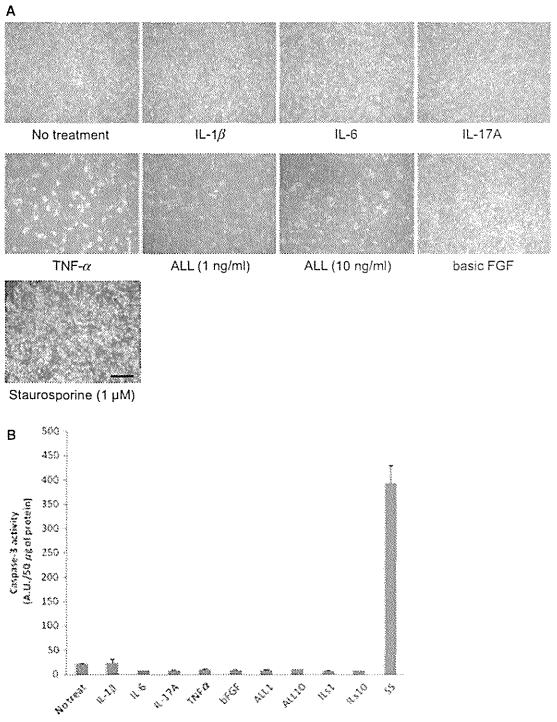

Figure 7. Proinflammatory cyotokines induce melanocyte cell destruction, but not apoptosis. (A) Human melanocytes were incubated with recombinant proinflammatory cytokines, including IL-1β, IL-6, IL-17A, and TNF-α continuously for 5 days at concentrations of 1 or 10 ng/ml in the culture medium. These cytokines were used either alone or in combination. Staurosporine was used as a positive control for cell apoptosis. The photographs were taken by a polarized microscope. The bar indicates 50 μm. (B) The absorbance at 450 nm was measured to determine the caspase-3 activity of the cells treated with cytokines. ILs indicates treatment together with IL-1β, IL-6 and IL-17A.

genesis and melanocyte survival (Moretti et al., 2002, 2009).

Direct regulation of melangenic factors by cytokines

The tyrosinase mRNA levels are generally correlated with tyrosinase activity (Ando et al., 1995). In our study, cytokine treatment decreased the mRNA levels of MITF, a transcription factor implicated in regulating melanogenic and antiapoptotic genes, and decreased the expression of genes encoding melanogenic enzymes such as tyrosinase, TYRP-1, and DCT (TYRP-2) in a dose-dependent manner. These results indicate that proinflammatory cytokines can play a pivotal role in the regulation of melanocyte fate through the downregulation of gene expression.

There have been several reports providing evidence that melanocyte functions are regulated by cytokines *through several cellular signaling pathways* (Kamaraju et al., 2002; Kholmanskikh et al., 2010). For example, IL-1β and 1α were found to direct the downregulation of MITF-M expression through the NF-κB and JNK pathways in two different melanoma cell lines (Kholmanskikh et al., 2010). IL-6/IL-6R signaling silenced the MITF promoter activity and this was mediated by Pax3 downregulation (Kamaraju et al., 2002). IL-6 is a pleiotropic cytokine involved in a variety of inflammatory responses. With regard to the relationship to Th17 cells, IL-6 is essential for induction of Th17 cell development and maintenance (Diveu et al., 2008). As the proinflammatory cytokines involved in Th17 cell fate include IL-1β and TGF-β in addition to IL-6, we examined the expression and activity of some of these cytokines in melanocytes.

Although there is no doubt that cellular and antibody-mediated immune reactions are related to melanocyte destruction, our data suggest that Th17 cells and skin-resident cells, particularly epidermal keratinocytes and *dermal fibroblasts, might orchestrate a response that* inhibits the stability of melanocytes in some vitiligo skin

through the production of proinflammatory cytokines. In addition, there might be an initial trigger attracting Th17 cells to vitiligo (or pre-vitiligo) skin.

A recent study using several skin samples showed greater numbers of Th17 cells, especially on the leading edge of vitiligo skin (Wang et al., 2011). In the present study, we confirm the presence of Th17 cell infiltration in vitiligo skin and suggest that there was a pathogenic function not only because of cytotoxic T cells but also because of Th17 cells and Th17 cell-related cytokines. Although we expected that there would be more infiltration of Th17 cells in the generalized type and progressive vitiligo compared with other clinical types, there was no significant correlation between the Th17 cell number and the clinical type and disease duration. It is possible that the small sample number, biopsy site, and preceding treatments, including the use of topical steroids, may have affected the status of inflammatory cell infiltration.

We observed that Th17 cells diffusely infiltrated the upper dermis, whereas $CD8^+$ cells were present beneath the basal membrane of the epidermis. In psoriatic skin, Th17 cells mainly infiltrate into the papillary dermis and epidermis. We therefore speculated that Th17 cells might be able to act on melanocytes by producing cytokines, rather than exerting a direct effect on the cells. To address this point, we stimulated dermal fibroblasts and keratinocytes using a characteristic pro-Th17 cytokine, IL-17A. IL-17A robustly upregulated the production of IL-1β and TNF-α by these skin-resident cells, suggesting the presence of mutual cytokine signaling between skin-resident cells and accumulating inflammatory cells. The melanocytes themselves can also synthesize IL-1α and β (Swope et al., 1994).

Previous studies have shown that cytokines associated with skin inflammation, such as IL-1β, IL-6, and TNF-α, inhibited melanin production in vitro (Englaro et al., 1999; Kamaraju et al., 2002; Kholmanskikh et al., 2010). We found that there were significant changes in the expression of epidermal cytokines in vitiligo lesions, where no melanocytes are present, compared with perilesional, non-lesional and healthy skin, where melanocytes are normally present. Therefore, it is conceivable that the cytokines derived from infiltrating cells, as well as the lesional epidermis, would be implicated in depigmented skin disorders. In the present study, treatment with a physiologically relevant concentration of IL-17A, in addition to IL-1β and IL-6, could directly regulate the expression of MITF and downstream molecules, and subsequently melanin synthesis, in human melanocytes.

Putative involvement of proinflammatory cytokines in vitiligo

Based on these experimental results, we propose the putative involvement of proinflammatory cytokines in the pathogenesis of vitiligo (Figure 8). Previous studies have shown that the perforin produced from CD8-positive cytotoxic T cells (Lang et al., 2001; Norris et al., 1994; Ogg et al., 1998), antimelanocyte antibodies (Baharav et al., 1996; Cui et al., 1992; Ruiz-Arguelles et al., 2007), and reactive oxygen species were related to the injury of melanocytes and were triggers for vitiligo (Schallreuter et al., 1994b). In the present study, we found a significant infiltration of Th17 cells in vitiligo skin, and demonstrated that Th17-related cytokines such as IL-1β, IL-6, and IL-17A directly or indirectly regulated melanin production and the expression of melanogenic and antiapoptotic molecules. The presence of a cytokine network and the secretion of IL-17A from Th17 cells may therefore represent a new mechanism underlying the pathogenesis of vitiligo concerning the downregulation of melanocyte activity. Indeed, the activation of the innate immune system may lead to the accumulation of Th17 cells in the vitiligo lesion as they do in psoriasis. In fact, the IL-1β released from lesional keratinocytes and melanocytes (Moretti et al., 2002, 2009; Swope et al., 1994) may act as the first inducer of the differentiation of naïve helper T cells into Th17 cells in vitiligo lesions. Thereafter, antimicrobial peptides derived from the lesional epidermis might induce the production of IL-17A by Th17 cells (Infante-Duarte et al., 2000).

Although psoriasis is one of representative skin disorders characterized by pathogenic Th17 cell infiltration, the phenotypic change in this disorder is not akin to that in vitiligo vulgaris. Because the final targets of IL-17A in

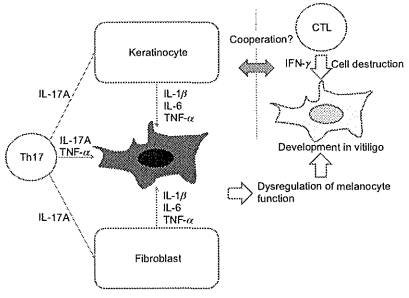

Figure 8. The proposed cues provided by Th17 cells and Th17 cell-related cytokines during the pathogenesis of autoimmune vitiligo. Previous known pathogenic mechanisms of melanocyte destruction in vitiligo include the presence of cytotoxic T cells attacking the melanocytes, local oxidative stress, and downregulation of melanogenesis-inducing factors in the vitiligo epidermis. The newly proposed phenomenon is that an imbalance in the local cytokine network is involved in the downregulation of melanocyte activity found in the present study. The IL-17A secreted from the Th17 cells in vitiligo skin can trigger the production of inhibitory cytokines from dermal fibroblasts and keratinocytes. IL-1β, IL-6, and TNF-α as well as IL17-A also repress melanocyte activity and induce melanocyte destruction.

vitiligo vulgaris and psoriasis are different, that is, melanocyte dysfunction in vitiligo vulgaris and abnormal keratinocyte turnover in psoriasis, Th17 cells may augment vitiliginous skin lesion formation in cooperation with skin-resident cells such as dermal fibroblasts and keratinocytes, as described previously. Microbial lipopeptides may then induce the cell polarization to Th17 cells, producing IL-17 and TNF-α as a result of the stimulation of the innate immune system in vitiligo (Infante-Duarte et al., 2000). Tip dendritic cell (tipCD)-like cells might also be involved in vitiligo formation, as previous reports demonstrated that the number of αDCs was increased in vitiligo vulgaris lesions or there was a unique distribution pattern of Langerhans cells present in such lesions (Mishima et al., 1972). Moreover, recent reports suggest that an altered innate immune response is observed in autoimmune vitiligo in concert with frequent *NALP1* gene mutations (Jin et al., 2007, 2010). An unrecognized micro-organism might stimulate the attending inflammatory cells through antimicrobial peptides and sequentially trigger vitiligo vulgaris. These issues should be clarified in further experiments.

Methods

Cell lines

HeMnMP, a moderately pigmented human melanocyte cell line, was obtained from Cascade Biologics and cultured in Medium 254 with human melanocyte growth supplement (Gibco Inc., Tokyo, Japan), and maintained at 37°C with 5% CO_2 in a humidified incubator. The cells were used for this study by the 5th passage to ensure melanin production. Dermal fibroblasts and epidermal keratinocytes were purchased from TAKARA BIO Inc., (Shiga, Japan) and maintained in DMEM containing 10% FCS and Medium 154 (Gibco Inc.), respectively.

Reagents

Human recombinant cytokines were purchased from Cell Signaling Technology (Tokyo, Japan) and synthetic melanin was from Sigma-Aldrich, Japan. The antibodies used for this study were as follows: anti-MITF mouse monoclonal Ab (D5) from Abcam (San Francisco, CA, USA), horseradish peroxidase (HRP)-conjugated anti-rabbit or mouse IgG from Cell Signaling Technology, anti-CD4 mouse monoclonal antibody from Novocastra Reagents (Tokyo, Japan), anti-CD8, -Foxp3, -CD20 and -Melan A mouse monoclonal antibodies from Dako (Tokyo, Japan), anti-IL17A goat monoclonal antibody from R&D (Minneapolis, MN, USA), Alexa Fluor 488-conjugated anti-mouse IgG and Alexa Fluor 555-conjugated anti-goat IgG from Invitrogen (Tokyo, Japan).

Tissue specimens

Approval for the use of human skin tissue samples was obtained from the local Ethical Committee of Osaka University Hospital and written informed consent was received from each patient after appropriate explanation of this study. Spindle-shaped skin biopsy specimens on the leading edge of vitiligo lesions were taken from 23 vitiligo patients. Twenty-three skin specimens were fixed in buffered 10% formalin and embedded in paraffin and processed for an immunohistochemical analysis as described below. Non-lesional skin from the matched vitiligo patients and normal skin from normal donors were processed as well.

RNA isolation and PCR assay for cytokine and melanocyte markers expression

Total RNA was extracted from HeMnMP cells using the TRIZOL reagent according to the manufacturer's instructions. Reverse transcription (RT) reactions were performed with Moloney murine leukemia virus reverse transcriptase (Promega, Tokyo, Japan) with oligo (dT) primers. For RT reaction of tissue RNA, total RNA was extracted from frozen vilitigo skin tissue using the Sepasol-RNA I reagent (NACALAI TESQUE, INC., Kyoto, Japan) according to the manufacturer's instructions. Genomic DNA contamination was removed by DNase I (TAKARA BIO INC.). The qRT assay was performed using an ABI prism 7900HT Sequence Detection System (Applied Biosystems, Carlsbad, CA, USA) according to the manufacturer's specifications. Briefly, the reaction mixture totaling 10 μl for each qRT consisted of 1 μl of cDNA generated from 250 ng of total RNA, 0.5 μM of Taqman probe labeled with FAM, the master mix for melanogenic markers and glyceraldehyde 3-phosphate dehydrogenase (GAPDH), or the Power SYBR green PCR master mix for cytokines. The mixture was processed by a two-step PCR method with an initial heating at 95°C for 10 min, followed by 40 cycles of denaturation at 95°C for 15 s, and annealing and extension at 60°C for 60 s for all genes. The obtained PCR amplification curves were analyzed using SDS software program, version 2.1 (Applied Biosystems). GAPDH was used as a control housekeeping gene, and the relative mRNA copy numbers were obtained as the ratio of the mRNA copies of each gene/copies of GAPDH. Each assay was performed at least three times. The specific probe and primers sequences used for this study were as follows:

MITF-M: 5′-AGCTCACAGCGTGTATTTTTCCCAC-3′
TYR: 5′-TCTCCTCTTGGCAGATTGTCTGTAG-3′
TRP-1: 5′-CTTTGTAACAGCACCGAGGATGGGC-3′
DCT: 5′-TGCAAGTGCACAGGAAACTTTGCCG-3′
BCL2: 5′-AACGGAGGCTGGGATGCCTTTGTGG-3′
GAPDH: 5′-GGGCGCCTGGTCACCAGGGCTGCTT-3′
IL-1β: Forward 5′- TGCACGCTCCGGGACTCACA-3′
IL-1 β: Reverse 5′- CGCCTTTGGTCCCTCCCAGG-3′
TNF-α: Forward 5′- CCCCTGACAAGCTGCCAGGC-3′
TNF-α: Reverse 5′- CAGCTCCACGCCATTGGCCA-3′

Reverse transcriptase PCR (RT-PCR) for IL-17A and cytokine receptor expression

To confirm IL-17A expression in vitiligo tissue and determine the expression levels of the cytokines and their receptors, we performed RT reactions with the above-mentioned procedure and PCR with an initial heating at 95°C for 10 min, followed by 40 cycles of denaturation at 95°C for 15 s, and annealing and extension at appropriate temperatures for 60 s for all genes. Samples were then processed for electrophoresis. The following primer sets were used:

IL-17A: Forward 5′- ACAAACTCATCCATCCCCAG-3′
IL-17A: Reverse 5′- GTGAGGTGGATCGGTTGTAG-3′
IL-1R1: Forward 5′-CCCGTTGCAGGAGACGGAGG-3′
IL-1R1: Reverse 5′-CCACCCAGCCAGCTGAAGCC-3′
IL-1R2: Forward 5′-CTTTAAAGCTGCTTCTGCCACGTG-3′
IL-1R2: Reverse 5′-CATTGCCCGTCCACCACAGCA-3′
IL-6R: Forward 5′-GAGTTCGGGCAAGGCGAGTGG-3′
IL-6R: Reverse 5′-AGGCTCCCTCCAGCAACCAGGAA-3′
IL-17RA: Forward 5′-AAGCCTCAGAACGTTCGTTCGCT-3′
IL-17RA: Reverse 5′-TTGGGCAGGTGGTGAACGGT-3′

Melanin content assay

Melanin production was determined as described previously (Virador et al., 1999). Briefly, 2 days after the plating of 1×10^5 melanocytes into a 6-well culture dish, we performed 5 days of

sequential treatment with 1–10 ng/ml of recombinant cytokines. To determine the melanin content, the pellets of treated cells were dissolved in 200 μl of 1 N NaOH for 30 min, and the concentrations of melanin were calculated by measuring the absorbance at 450 nm. Synthetic melanin was used to generate a standard curve. The melanin content was expressed as nanograms of melanin per microgram of total protein, and the ratio was compared among the samples.

Immunostaining

Vitiliginous skin specimens were processed after receiving written informed consent from vitiligo patients (n = 23). Paraffin-embedded archival tissues were deparaffinized with absolute xylene and dehydrated in a sequential ethanol dilution series. The deparaffinized sections were boiled in an oil bath for 15 min in 10 mM Tris-1 mM EDTA buffer (pH 9.0) for antigen retrieval. The slides were blocked by the Protein Block Serum-Free solution (Dako) for 15 min and incubated with an anti-IL-17A goat monoclonal Ab (×200) at 4°C overnight. After being washed with TBS (pH 7.6), the slides were incubated with Alexa Fluor 555-conjugated anti-goat IgG Ab (×200) and then incubated with anti-CD4 mouse monoclonal Ab (×25) at RT for 1 h, followed by incubation with Alexa Fluor 488-conjugated anti-mouse IgG Ab (×200). The following primary antibodies were used to assess the expression of melanocyte markers and the melanosomal protein MART1: anti-CD8 mouse monoclonal Ab (×25), anti-CD20 mouse monoclonal Ab (×25), anti-Foxp3 mouse monoclonal Ab (×50), and anti-Melan A (recognizing the MART-1 antigen) mouse monoclonal Ab (×50). These antibodies were provided by DAKO Inc.

For the immunocytochemistry analyses, the HeMnMP cells cultured in two-well Lab-Tek chamber slides (Nunc, Tokyo, Japan) were incubated with an anti-MITF mouse monoclonal antibody (×25) at 4°C overnight, followed by incubation with Alexa Fluor 555-conjugated anti-mouse IgG (×500) as the secondary antibody. The mouse isotype IgG was used as a negative control for staining. Nuclei were counterstained after DAPI staining (×1000).

Quantitative analysis of proinflammatory cytokines after the treatment with Th17-related cytokines

To assess the cell–cell interactions between the cells in the skin occurring as a result of paracrine cytokine production, the concentrations of proinflammatory cytokines such as IL-6 and IL-1β in the culture supernatant from dermal fibroblasts was measured 24 h after treatment with recombinant IL-17A using an ELISA kit from R&D.

Apoptosis assay

We determined the cleaved caspase-3 activity following treatment with recombinant cytokines using an apoptosis detection kit (R&D Systems). Briefly, cultured melanocytes were treated with cytokines (1 or 10 ng/ml) for 5 days. The culture medium was not changed until cell extraction, and cytokines were added in the culture medium every day. Thereafter, in addition to observation of melanocyte morphology under a polarized microscope, the melanocytes were processed for measurement of cleaved caspase-3 activity according to manufacturer's instructions.

Statistical analysis

The unpaired *t*-test was used for the analysis of differences in gene and protein expression. The results are shown as the means + SD. A value of $P < 0.05$ (two-tailed) was considered significant. All statistical analyses were performed using the PRISM software program, version 5 (GraphPad Software Inc., La Jolla, CA, USA).

Acknowledgements

We thank Kenju Nishida, Eriko Nobuyoshi, and Tomoka Matsumura for their expert technical assistance. This work was supported in part by a grant from the Ministry of Education, Culture, Sports, Science and Technology of Japan and a grant from the Ministry of Health, Labor and Welfare.

References

Ando, H., Itoh, A., Mishima, Y., and Ichihashi, M. (1995). Correlation between the number of melanosomes, tyrosinase mRNA levels, and tyrosinase activity in cultured murine melanoma cells in response to various melanogenesis regulatory agents. J. Cell. Physiol. *163*, 608–614.

Asarch, A., Barak, O., Loo, D.S., and Gottlieb, A.B. (2008). Th17 cells: a new therapeutic target in inflammatory dermatoses. J. Dermatolog. Treat. *19*, 318–326.

Baharav, E., Merimski, O., Shoenfeld, Y., Zigelman, R., Gilbrud, B., Yecheskel, G., Youinou, P., and Fishman, P. (1996). Tyrosinase as an autoantigen in patients with vitiligo. Clin. Exp. Immunol. *105*, 84–88.

Basak, P.Y., Adiloglu, A.K., Ceyhan, A.M., Tas, T., and Akkaya, V.B. (2009). The role of helper and regulatory T cells in the pathogenesis of vitiligo. J. Am. Acad. Dermatol. *60*, 256–260.

Bassiouny, D.A., and Shaker, O. (2011). Role of interleukin-17 in the pathogenesis of vitiligo. Clin. Exp. Dermatol. *36*, 292–297.

Caixia, T., Hongwen, F., and Xiran, L. (1999). Levels of soluble interleukin-2 receptor in the sera and skin tissue fluids of patients with vitiligo. J. Dermatol. Sci. *21*, 59–62.

Chalraborty, A., and Pawelek, J. (1993). MSH receptors in immortalized human epidermal keratinocytes: a potential mechanism for coordinate regulation of the epidermal-melanin unit. J. Cell. Physiol. *157*, 344–350.

Cui, J., Harning, R., Henn, M., and Bystryn, J.C. (1992). Identification of pigment cell antigens defined by vitiligo antibodies. J. Invest. Dermatol. *98*, 162–165.

Daneshpazhooh, M., Mostofizadeh, G.M., Behjati, J., Akhyani, M., and Robati, R.M. (2006). Anti-thyroid peroxidase antibody and vitiligo: a controlled study. BMC Dermatol. *6*, 3.

Diveu, C., Mcgeachy, M.J., and Cua, D.J. (2008). Cytokines that regulate autoimmunity. Curr. Opin. Immunol. *20*, 663–668.

Englaro, W., Bahadoran, P., Bertolotto, C., Busca, R., Derijard, B., Livolsi, A., Peyron, J.F., Ortonne, J.P., and Ballotti, R. (1999). Tumor necrosis factor alpha-mediated inhibition of melanogenesis is dependent on nuclear factor kappa B activation. Oncogene *18*, 1553–1559.

Fitch, E.L., Rizzo, H.L., Kurtz, S.E., Wegmann, K.W., Gao, W., Benson, J.M., Hinrichs, D.J., and Blauvelt, A. (2009). Inflammatory skin disease in K5.hTGF-beta1 transgenic mice is not dependent on the IL-23/Th17 inflammatory pathway. J. Invest. Dermatol. *129*, 2443–2450.

Gould, I.M., Gray, R.S., Urbaniak, S.J., Elton, R.A., and Duncan, L.J. (1985). Vitiligo in diabetes mellitus. Br. J. Dermatol. *113*, 153–155.

Hegedus, L., Heidenheim, M., Gervil, M., Hjalgrim, H., and Hoier-Madsen, M. (1994). High frequency of thyroid dysfunction in patients with vitiligo. Acta Derm. Venereol. *74*, 120–123.

Howitz, J., Brodthagen, H., Schwartz, M., and Thomsen, K. (1977). Prevalence of vitiligo. Epidemiological survey on the Isle of Bornholm, Denmark. Arch. Dermatol. *113*, 47–52.

Infante-Duarte, C., Horton, H.F., Byrne, M.C., and Kamradt, T. (2000). Microbial lipopeptides induce the production of IL-17 in Th cells. J. Immunol. *165*, 6107–6115.

Jin, Y., Mailloux, C.M., Gowan, K., Riccardi, S.L., Laberge, G., Bennett, D.C., Fain, P.R., and Spritz, R.A. (2007). NALP1 in vitiligo-associated multiple autoimmune disease. N. Engl. J. Med. *356*, 1216–1225.

Jin, Y., Riccardi, S.L., Gowan, K., Fain, P.R., and Spritz, R.A. (2010). Fine-mapping of vitiligo susceptibility loci on chromosomes 7 and 9 and interactions with NLRP1 (NALP1). J. Invest. Dermatol. *130*, 774–783.

Kamaraju, A.K., Bertolotto, C., Chebath, J., and Revel, M. (2002). Pax3 down-regulation and shut-off of melanogenesis in melanoma B16/F10.9 by interleukin-6 receptor signaling. J. Biol. Chem. *277*, 15132–15141.

Kholmanskikh, O., Van Baren, N., Brasseur, F., Ottaviani, S., Vanacker, J., Arts, N., Van Der Bruggen, P., Coulie, P., and De Plaen, E. (2010). Interleukins 1alpha and 1beta secreted by some melanoma cell lines strongly reduce expression of MITF-M and melanocyte differentiation antigens. Int. J. Cancer *127*, 1625–1636.

Kingo, K., Aunin, E., Karelson, M., Ratsep, R., Silm, H., Vasar, E., and Koks, S. (2008). Expressional changes in the intracellular melanogenesis pathways and their possible role in the pathogenesis of vitiligo. J. Dermatol. Sci. *52*, 39–46.

Kolls, J.K., and Linden, A. (2004). Interleukin-17 family members and inflammation. Immunity *21*, 467–476.

Lang, K.S., Caroli, C.C., Muhm, A., Wernet, D., Moris, A., Schittek, B., Knauss-Scherwitz, E., Stevanovic, S., Rammensee, H.G., and Garbe, C. (2001). HLA-A2 restricted, melanocyte-specific CD8(+) T lymphocytes detected in vitiligo patients are related to disease activity and are predominantly directed against MelanA/MART1. J. Invest. Dermatol. *116*, 891–897.

Levy, C., Khaled, M., and Fisher, D.E. (2006). MITF: master regulator of melanocyte development and melanoma oncogene. Trends Mol. Med. *12*, 406–414.

Liang, S.C., Tan, X.Y., Luxenberg, D.P., Karim, R., Dunussi-Joannopoulos, K., Collins, M., and Fouser, L.A. (2006). Interleukin (IL)-22 and IL-17 are coexpressed by Th17 cells and cooperatively enhance expression of antimicrobial peptides. J. Exp. Med. *203*, 2271–2279.

Mihailova, D., Grigorova, R., Vassileva, B., Mladenova, G., Ivanova, N., Stephanov, S., Lissitchky, K., and Dimova, E. (1999). Autoimmune thyroid disorders in juvenile chronic arthritis and systemic lupus erythematosus. Adv. Exp. Med. Biol. *455*, 55–60.

Mishima, Y., Kawasaki, H., and Pinkus, H. (1972). Dendritic cell dynamics in progressive depigmentations. Distinctive cytokinetics of -dendritic cells revealed by electron microscopy. Arch. Dermatol. Forsch. *243*, 67–87.

Moretti, S., Spallanzani, A., Amato, L., Hautmann, G., Gallerani, I., Fabiani, M., and Fabbri, P. (2002). New insights into the pathogenesis of vitiligo: imbalance of epidermal cytokines at sites of lesions. Pigment Cell Res. *15*, 87–92.

Moretti, S., Fabbri, P., Baroni, G., Berti, S., Bani, D., Berti, E., Nassini, R., Lotti, T., and Massi, D. (2009). Keratinocyte dysfunction in vitiligo epidermis: cytokine microenvironment and correlation to keratinocyte apoptosis. Histol. Histopathol. *24*, 849–857.

Norris, D.A., Horikawa, T., and Morelli, J.G. (1994). Melanocyte destruction and repopulation in vitiligo. Pigment Cell Res. *7*, 193–203.

Ogg, G.S., Rod Dunbar, P., Romero, P., Chen, J.L., and Cerundolo, V. (1998). High frequency of skin-homing melanocyte-specific cytotoxic T lymphocytes in autoimmune vitiligo. J. Exp. Med. *188*, 1203–1208.

Okamoto, T., Irie, R.F., Fujii, S., Huang, S.K., Nizze, A.J., Morton, D.L., and Hoon, D.S. (1998). Anti-tyrosinase-related protein-2 immune response in vitiligo patients and melanoma patients receiving active-specific immunotherapy. J. Invest. Dermatol. *111*, 1034–1039.

Ongenae, K., Van Geel, N., and Naeyaert, J.M. (2003). Evidence for an autoimmune pathogenesis of vitiligo. Pigment Cell Res. *16*, 90–100.

Ratsep, R., Kingo, K., Karelson, M., Reimann, E., Raud, K., Silm, H., Vasar, E., and Koks, S. (2008). Gene expression study of IL10 family genes in vitiligo skin biopsies, peripheral blood mononuclear cells and sera. Br. J. Dermatol. *159*, 1275–1281.

Ruiz-Arguelles, A., Brito, G.J., Reyes-Izquierdo, P., Perez-Romano, B., and Sanchez-Sosa, S. (2007). Apoptosis of melanocytes in vitiligo results from antibody penetration. J. Autoimmun. *29*, 281–286.

Schallreuter, K.U., Lemke, R., Brandt, O., Schwartz, R., Westhofen, M., Montz, R., and Berger, J. (1994a). Vitiligo and other diseases: coexistence or true association? Hamburg study on 321 patients. Dermatology *188*, 269–275.

Schallreuter, K.U., Wood, J.M., Pittelkow, M.R., Gutlich, M., Lemke, K.R., Rodl, W., Swanson, N.N., Hitzemann, K., and Ziegler, I. (1994b). Regulation of melanin biosynthesis in the human epidermis by tetrahydrobiopterin. Science *263*, 1444–1446.

Swope, V.B., Sauder, D.N., Mckenzie, R.C., Sramkoski, R.M., Krug, K.A., Babcock, G.F., Nordlund, J.J., and Abdel-Malek, Z.A. (1994). Synthesis of interleukin-1 alpha and beta by normal human melanocytes. J. Invest. Dermatol. *102*, 749–753.

Virador, V.M., Kobayashi, N., Matsunaga, J., and Hearing, V.J. (1999). A standardized protocol for assessing regulators of pigmentation. Anal. Biochem. *270*, 207–219.

Wang, C.Q., Cruz-Inigo, A.E., Fuentes-Duculan, J., Moussai, D., Gulati, N., Sullivan-Whalen, M., Gilleaudeau, P., Cohen, J.A., and Krueger, J.G. (2011). Th17 cells and activated dendritic cells are increased in vitiligo lesions. PLoS ONE *6*, e18907.

Wilson, N.J., Boniface, K., Chan, J.R. et al. (2007). Development, cytokine profile and function of human interleukin 17-producing helper T cells. Nat. Immunol. *8*, 950–957.

Supporting information

Additional Supporting Information may be found in the online version of this article:

Figure S1. Coculture of helper T cells and melanocytes, and measurement of the expression of melanogenic markers.

Please note: Wiley-Blackwell are not responsible for the content or functionality of any supporting materials supplied by the authors. Any queries (other than missing material) should be directed to the corresponding author for the article.

EXD 1454 B
Journal Name Manuscript No.
Dispatch: 3.2.12 Journal: EXD CE: Deepika K
Author Received: No. of pages: 6 PE: Sathya Kala

DOI:10.1111/j.1600-0625.2012.01454.x
www.blackwellpublishing.com/EXD

Original Article

Periostin, a matricellular protein, accelerates cutaneous wound repair by activating dermal fibroblasts

Kanako Ontsuka[1*], Yorihisa Kotobuki[2,3*], Hiroshi Shiraishi[1], Satoshi Serada[3], Shoichiro Ohta[4], Atsushi Tanemura[2], Lingli Yang[2,3], Minoru Fujimoto[3], Kazuhiko Arima[1], Shoichi Suzuki[1], Hiroyuki Murota[2], Shuji Toda[5], Akira Kudo[6], Simon J. Conway[7], Yutaka Narisawa[8], Ichiro Katayama[2], Kenji Izuhara[1] and Tetsuji Naka[3]

[1]Division of Medical Biochemistry, Department of Biomolecular Sciences, Saga Medical School, Saga, Japan; [2]Department of Dermatology, Osaka University Graduate School of Medicine, Suita, Japan; [3]Laboratory for Immune Signal, National Institute of Biochemical Innovation, Ibaraki, Japan; [4]Department of Laboratory Medicine, Saga Medical School, Saga, Japan; [5]Department of Pathology and Biodefense, Saga Medical School, Saga, Japan; [6]Department of Biological Information, Tokyo Institute of Technology, Yokohama, Japan; [7]Program in Developmental Biology and Neonatal Medicine, Herman B. Wells Center for Pediatric Research, Indiana University School of Medicine, Indianapolis, IN, USA; [8]Department of Dermatology, Saga Medical School, Saga, Japan

Correspondence: Kenji Izuhara, Division of Medical Biochemistry, Department of Biomolecular Sciences, Saga Medical School, 5-1-1, Nabeshima, Saga 849-8501, Japan, Tel.: +81-952-34-2261, Fax: +81-952-34-2058, e-mail: kizuhara@cc.saga-u.ac.jp

**These two authors contributed equally to this work.*

Abstract: Cutaneous wound repair is a highly ordered and well-coordinated process involving various cell lineages and many molecular effectors. Cell–matrix interactions through integrin molecules provide key signals important for wound repair. Periostin is a matricellular protein that may provide signals important during tissue development and remodelling by interacting with several integrin molecules, via the phosphatidylinositol 3-kinase/Akt and MAP kinase pathways. In this study, we examined the role of periostin in the process of cutaneous wound repair using periostin-deficient mice and by analysing the effects of periostin on dermal fibroblasts. We first determined the expression profile and localization of periostin in a well-characterized wound repair model mice. Periostin was robustly deposited in the granulation tissues beneath the extended epidermal wound edges and at the dermal–epidermal junctions in wounded mice. Moreover, periostin-deficient mice exhibited delayed *in vivo* wound repair, which could be improved by direct administration of exogenous periostin. *In vitro* analyses revealed that loss of periostin impaired proliferation and migration of dermal fibroblasts, but exogenous supplementation or enforced periostin expression enhanced their proliferation. Combined, these results demonstrate that periostin accelerates the process of cutaneous wound repair by activating fibroblasts.

Key words: fibroblast – matrix – mice – periostinintegrin – wound repair

Accepted for publication 18 January 2012

Introduction

Cutaneous wound repair is a physiological function that is well ordered and highly coordinated (1–4). The process of repair is divided into three phases: inflammation, new tissue formation and remodelling. In the inflammatory phase beginning with haemostasis, first neutrophils and later macrophages are recruited to the wound site. These infiltrated macrophages not only exert their phagocytic activities but also accelerate re-epithelialization and granulation tissue formation. During new tissue formation, the process of re-epithelialization occurs via extension of wedge-shaped keratinocyte lineage. Fibroblasts and macrophages subsequently form the granulation tissues, assisting in the key process of re-epithelialization. Finally, during the remodelling phase, most of the endothelial cells, macrophages and myofibroblasts undergo apoptosis, leaving a scar containing a few cells with an extensive extracellular matrix (ECM) deposition dominated by collagens.

In the new tissue forming phase, fibroblasts produce mainly collagens and other ECM components such as glycosaminoglycans and proteoglycans, contributing to the formation of granulation tissues, with the provisional fibrin-based matrix eventually being replaced (1,5–7). In addition, fibroblasts secrete various growth factors – fibroblast growth factor-2 (FGF-2)/basic FGF, FGF-7/keratinocyte growth factor, FGF-10, epidermal growth factor and transforming growth factor-β (TGF-β) – which can all affect the process of keratinocyte re-epithelialization (8). TGF-β1 can also drive differentiation of some fibroblasts into transformed myofibroblasts that express α-smooth muscle actin (α-SMA) (9), which are able to contract to draw the wound edges together (1–4). This combination of growth factor receptor–mediated signals and integrin-mediated signals are thought to result in growth, migration, survival, spreading and ECM production responses within the wound fibroblasts (10–12). However, the underlying mechanism of fibroblast activation during cutaneous wound repair has not yet been fully understood.

Periostin is an ECM protein belonging to the fasciclin family (13,14) and is a newly characterized matricellular protein whose main functions are thought to be modulation of cell–matrix interactions and cell functions rather than playing a direct structural role (15,16). Periostin is known to interact with several integrin molecules, specifically $\alpha_v\beta_3$ or $\alpha_v\beta_5$ on cell surfaces, activating the phosphatidylinositol 3-kinase (PI3K)/Akt and MAP kinase pathways during tissue development and remodelling (13,14). We and others have demonstrated the presence of periostin in fibrotic areas in various pathological conditions: bronchial asthma (17–19), pulmonary fibrosis (20), myocardial infarction (21), valvular heart disease (22), cystic fibrosis (23) and proliferative diabetic retinopathy (24). Further, it has been shown that the biological functions of periostin as a matricellular protein rather than structural player are important for the pathogenesis of some of these diseases. For instance, periostin affects eosinophils and/or epithelial cells in bronchial asthma, enhancing eosinophil migration and/or activating TGF-β, respectively (25,26). Moreover, in the healing process of myocardial infarction, periostin may enhance cardiac repair via stimulation of myocyte proliferation (27), although whether this is a direct mechanism or via adjacent cardiac fibroblasts remains controversial (28). Furthermore, periostin accelerates the development of various tumors by promoting cancer cell survival, epithelial–mesenchymal transition, invasion and metastasis (29,30). In contrast, the physiological roles of periostin remain poorly understood, except for several studies using periostin-deficient mice that suggest non-replaceable roles for periostin during development of bone, tooth and heart valves (14,31).

Importantly for this study, periostin is known to be highly expressed in wounds, suggesting its involvement in the process of wound repair (32,33). To directly examine the role of periostin within the process of cutaneous wound repair, we employed both *in vivo* and *in vitro* approaches using systemic periostin-deficient mice, exogenous periostin supplementation and a well-characterized mouse wound repair model. Significantly, wound repair is delayed in periostin-deficient mice. Furthermore, exogenous periostin up-regulates proliferation and migration of the dermal fibroblasts, which suggests this may be the mechanism how periostin accelerates cutaneous wound repair. These results demonstrate that periostin is required for the process of cutaneous wound repair, highlighting its physiological role, and suggest that periostin may be a useful candidate to therapeutically speedup wound repair.

Methods

Mice

Eight- to twelve-week-old C57BL/6 or BALB/c mice (Japan SLC, Japan), periostin-deficient (*Postn*$^{-/-}$, C57BL/6 or BALB/c background) mice, were used (14,21). Experiments were undertaken following the guidelines for care and use of experimental animals required by the Japanese Association for Laboratory Animals Science (1987).

Mouse wound repair model

Mice were anaesthetized by inhalation of halothane or intraperitoneal injection of pentobarbital. After their backs were shaved, 8- or 10-mm diameter full-thickness wounds were generated using disposable biopsy punches (Kai Industries, Seki, Japan). Wound sizes were measured longitudinally with a slide calliper. Wound tissues were excised at indicated time points postinjury and used for quantitative RT-PCR, Western blotting or histological analysis. Following fixation in 3.7% formaldehyde and embedding in paraffin, histological analysis was performed on serial sections from spanning the central portion of the wound and stained with haematoxylin and eosin (H&E), Masson's trichrome and/or via immunohistochemical staining as previously described (18,20). In selected experiments, 2 μg recombinant mouse periostin (R&D Systems, Minneapolis, MN, USA) was painted onto the wound lesions every 2 days from day 1 to 9.

Quantitative RT-PCR

Quantitative RT-PCR was used to measure periostin as previously described (18). Briefly, RNA from wound site was isolated using an RNeasy Mini kit (Qiagen Japan, Tokyo, Japan), and the RT reaction was performed using a QuantiTect Reverse Transcription Kit (Qiagen Japan). Quantitative analysis was achieved using Applied Biosystems StepOnePlus™ Real-Time PCR System (Life Technologies Japan, Tokyo, Japan). The primer sequence and PCR conditions are referred to the Data S1.

Confocal microscopy

Excised wound tissues were fixed with 3.7% formaldehyde and embedded in paraffin. After blocking with 2% BSA, the wax sections were stained using polyclonal anti-periostin Ab, previously prepared (18) followed by Alexa488-labelled anti-rabbit IgG Ab (Invitrogen, Carlsbad, CA, USA). The sections were mounted by Dako fluorescent mounting medium (Dako, Glostrup, Denmark) and then examined by LSM5 PASCAL G/B microscope (Carl Zeiss Japan, Tokyo, Japan).

Transduction of periostin into MEFs

Mouse full-length *Postn* cDNA was cloned (ENSMUST000000-81564) from MEF. Overexpression of mouse periostin into wild-type or periostin-deficient MEFs was performed using retroviral transduction of pMXs-puro vector [provided by Dr. Toshio Kitamura, Tokyo University, Tokyo, Japan (34)]. As a control, an empty vector was used alongside periostin-containing vector. After transduction, only infected cells were selected by 1 μg/ml puromycin (InvivoGen, San Diego, CA, USA).

Proliferation assay

Proliferation of fibroblasts was examined using the Cell Counting Reagent SF (Nacalai Tesque, Kyoto, Japan) according to the manufacturer's recommendations. In selected experiments, after 4-h serum starvation, dermal fibroblasts were seeded on the specified concentration of recombinant periostin (as described previously).

Statistical analyses

The results are presented as means + SD. Analysis was carried out using the two-sided, unpaired Student's *t*-test or the two-sided Welch test. Multiple comparisons between groups were performed by Fisher's or Dunnett's methods. We considered values to be significant when $P < 0.05$.

Results

Periostin expression is induced in wound tissues

We first analysed the expression of periostin in wound tissues. In C57BL/6 mice, periostin mRNA started to increase at day 1 after injury and peaked at day 7, decreasing thereafter (Fig. 1a, $n = 8$). Correspondingly, periostin protein levels peaked at day 7–10 and were sustained until day 18 (Fig. 1b). Wounded mice on the BALB/c background showed almost identical kinetics of periostin temporal changes at both the mRNA and protein levels (Fig. S1, $n = 8$). We then examined whether the localization of periostin was altered in wounded tissues. In the normal unwounded skin, periostin was expressed weakly at the dermal–epidermal junction and relatively robustly around the hair follicles (Figs 1c and S2). At day 6, when the wound was still open with hypertrophic epidermal wound edges and granulation tissues formed beneath these edges, periostin was now strongly expressed in the dermal–epidermal junction at these edges and within the granulation tissues. At day 9, when the wound was closed, significant expression of periostin was still observed in the granulation tissues beneath

COLOR

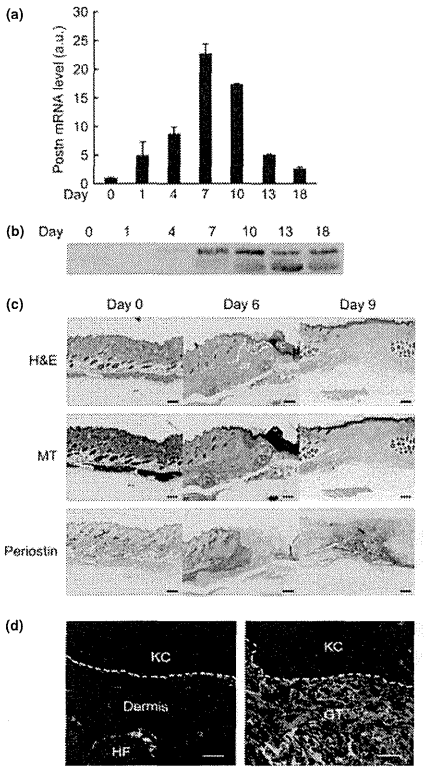

Figure 1. Periostin expression in wounded tissues. (a, b) Analysis of expression of periostin mRNA (a) or periostin protein (b) in wounded skin of C57BL/6 (n = 8) mice following the indicated amount of days postinjury. In b, experiments were repeated three times, and the representative combined data are depicted. (c) Wound sites stained with H&E, Masson trichrome (MT) and anti-periostin Ab from wild-type C57BL/6 mice for the indicated amount of days postinjury. FC, fibrin clot; EE, epidermal edge; GT, granulation tissue. Scale bar represents 200 μm. (d) Confocal microscopic imaging of wounds at day 6 is shown. Left and right panels depict non-wounded or wounded areas, respectively. Green and red represent periostin and the intrinsic fluorescence of cells, respectively. Scale bar represents 20 μm. KC, keratinocyte; GT, granulation tissue; HC, hair follicle.

the re-epithelialized wounds. To assess localization, we double-stained periostin (appears green), and this enabled us to conclude that periostin was deposited only at the border between the epidermis and the dermis and around hair follicles in the non-wounded sites, whereas periostin was deposited in the interspace regions of the red-staining granulation tissues in the wounded sites (Fig. 1d). These results demonstrate that periostin is induced during wound repair, suggesting that periostin may play a role in the repair process as well as being a useful marker of well-organized wound repair.

Periostin is required for efficient wound repair in mice

To test the functional requirement of periostin in wound repair, we used periostin-deficient ($Postn^{-/-}$) mice to perform wounding and assess their response. The wound sizes during the healing time course were significantly reduced in $Postn^{+/+}$ mice in C57BL/6 background (Fig. 2a,b, n = 10 for each genotype, $P < 0.05$ at day 3, 5 and 11, $P < 0.01$ at day 7) and in $Postn^{+/-}$ mice in a BALB/c background (Fig. S3, n = 3 for $Postn^{-/-}$ and n = 6 for $Postn^{+/-}$, $P < 0.05$ at day 3 and 10, $P < 0.001$ at day 13) than those observed in age-matched litter $Postn^{-/-}$ mice. Accordingly, the time intervals to completely close the wounds were significantly extended in $Postn^{-/-}$ mice than within $Postn^{+/+}$ mice (Fig. S4, 14.1 ± 0.74 days vs 15.9 ± 1.6 days, $P < 0.05$).

When we painted recombinant periostin protein onto the wounded area of $Postn^{-/-}$ mice every 2 days, starting day 1 after injury to day 9, the observed slower wound repair was subsequently accelerated (Fig. 2c,d upper panel, n = 10 for each group, the wound sizes: $P < 0.01$ at day 3, $P < 0.001$ at day 5 and 7, the time interval required to close the wounds: 15.9 ± 1.6 days vs 13.8 ± 1.4 days, $P < 0.01$). Moreover, the effects of administering exogenous periostin on accelerating wound repair were observed even in $Postn^{+/+}$ mice (Fig. 2c lower panel and Fig. S4, the wound sizes: $P < 0.05$ at day 7, the time interval to close the wounds: 14.1 ± 0.74 days vs 12.8 ± 1.1 days, $P < 0.01$). Thus, these results clearly demonstrate the requirement and positive effect of periostin within the wound repair process in mice.

Effect of periostin on proliferation in dermal fibroblasts

It has been shown that periostin can bind $\alpha_v\beta_3$ and $\alpha_v\beta_5$ integrin heterodimers (13,14) and that signalling via integrin molecules is imperative for cell proliferation and migration (10–12). Thus, we confirmed that α_v, β_3 and β_5 integrins, but not β_4 integrin, were expressed in human dermal fibroblasts, although A431 cells express β_4 integrin (Fig. S5A). Furthermore, when we stimulated human dermal fibroblasts with recombinant periostin, phosphorylation of downstream molecules of integrins focal adhesion kinase [FAK, STAT3, Akt and p44/42MAPK] was also observed (Fig. S5B). These results suggest that the interaction of periostin with human dermal fibroblasts is able to activate key signalling pathways via integrins present in the wound.

The present observation that periostin was strongly deposited within the granulation tissues beneath the hypertrophic epidermal wound edges raised the possibility that periostin may directly affect fibroblast proliferation, thereby accelerating the repair process. To explore this possibility, we initially examined the effects of exogenous periostin on proliferation of normal human dermal fibroblasts (NHDFs). We confirmed that NHDFs proliferate in response to FGF2 (Fig. S6). We also found that proliferation of NHDFs was up-regulated in a dose-dependent manner of periostin coated on plates (Fig. 3a, $P < 0.05$ at periostin 0.1 μg/ml, 24 h, $P < 0.01$ at periostin 1 μg/ml, 24 h, $P < 0.001$ at periostin 0.1 or 1 μg/ml, 72 h and at periostin 0.1 or 1 μg/ml, 120 h). We then analysed the effects of periostin deficiency on proliferative activities of mouse dermal fibroblasts. Fibroblast cultures established from skin of newborn $Postn^{-/-}$ mice had impaired proliferation compared with fibroblasts from $Postn^{+/+}$ mice (Fig. 3b, $P < 0.05$ at 6 and 48 h, $P < 0.01$ at 24 h, $P < 0.001$ at 72 h). Treatment

with recombinant periostin slightly enhanced proliferation of fibroblasts from both wild-type (Fig. 3c, $P < 0.05$ at 72 h) and periostin-deficient ($P < 0.05$ at 12 and 24 h) mice. Further, we overexpressed retrovirally periostin in periostin-deficient fibroblasts and in wild-type fibroblasts (Fig. S7). As expected, these periostin-overexpressed cells had significantly up-regulated proliferation compared with mock-transfected wild-type (Fig. 3d, $P < 0.001$ at 24, 48, 60 and 72 h) or periostin-deficient (Fig. 3d, $P < 0.01$ at 60 and 72 h, $P < 0.001$ at 24 and 48 h) fibroblasts, respectively. These *in vitro* data demonstrate that either exogenously added or ectopically expressed periostin enhances the proliferative activities of fibroblasts.

COLOR

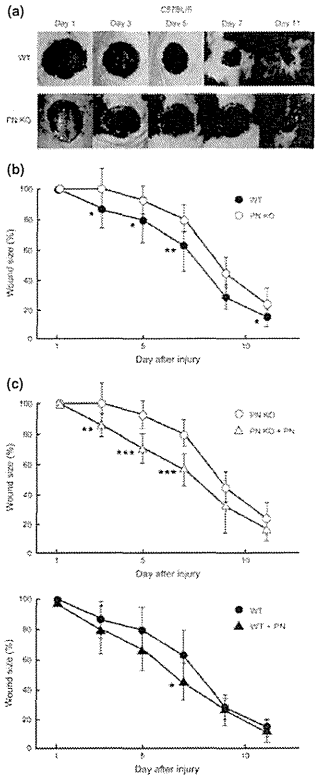

Figure 2. Periostin is important for efficient wound healing in mice. Successive photographs of the wounds (a), wound sizes at the indicated amount of days postinjury (b) in wild-type (WT, n = 10), or periostin-deficient mice (PN KO, n = 10) in C57BL/6 background. (c) Recombinant human periostin (+PN 2 μg) was injected intradermally into wounds of C57BL/6 background mice (n = 10 for each of WT and PN KO) every 2 days, from day 1 after injury to day 9. Wound sizes at the indicated times after injury (c). Statistical differences between PN KO vs WT, PN KO + PN vs PN KO and WT + PN vs WT are depicted. *$P < 0.05$, **$P < 0.01$, ***$P < 0.001$.

Respectively. These *in vitro* data demonstrate that either exogenously added or ectopically expressed periostin enhances the proliferative activities of fibroblasts.

Periostin enhances migration of dermal fibroblasts

We then examined the effects of periostin on migration of dermal fibroblasts using scratch wound cell monolayer method in wild-type and periostin-deficient MEFs (Fig. 4a,b). To exclude confounding effects upon proliferation, we arrested cell growth prior to analysis of migration. We confirmed that the migration activity of wild-type MEFs was up-regulated by platelet-derived growth factor (PDGF), whereas that was down-regulated by cytochalasin D (Fig. S8). The motility of periostin-deficient MEFs was significantly impaired compared with that of wild-type MEFs ($P < 0.05$ at 24 h). These results demonstrate that periostin can also enhance migration as well as the proliferation status of fibroblasts in response to wounding.

Discussion

It is well recognized that the ECM regulates the functions of the various cell lineages mobilized to the wounded area, contributing not only to re-epithelialization but also to granulation tissue formation and angiogenesis (35). Moreover, several studies using genetically deficient mice have shown that ECM proteins can play important *in vivo* functions during wounding and repair. For instance, fibronectin and its co-receptor, syndecan-4, are thought to accelerate wound repair as loss-of-function mouse mutants defective in the extra domain A of fibronectin or syndecan-4 both exhibit delayed cutaneous wound repair (36,37), whereas thrombospondin-1 and -2 play an opposite role and mainly inhibit wound repair (38,39). Based on previous observations that periostin is an ECM protein highly expressed during wound repair in various mouse models (32,33), in this study, we used periostin-deficient mice to test its requirement via our wound repair model. Meaningfully, both *in vivo* and *in vitro* results support the conclusion that periostin accelerates the wound healing process. Recently, using periostin-deficient mice, Nishiyama et al. (40) also reported that lack of periostin delays the process of cutaneous wound repair. Taking these results together, the requirement of periostin for the process of efficient cutaneous wound repair is well established.

The Nishiyama et al. (40) data indicated that periostin up-regulates keratinocyte proliferation and migration, accelerating the process of re-epithelialization. This result is consistent with our observation of significant periostin expression observed in the dermal–epidermal junction during wound repair. In our study, we similarly demonstrate that periostin enhances proliferation and migration of fibroblasts, which would contribute to the process of granulation tissue formation. We also demonstrated that periostin is deposited in fibroblast-enriched granulation tissues. Fibroblasts contribute to wound repair by generating several growth factors important for re-epithelialization (8) and by differentiating into α-SMA-expressing myofibroblasts important to close the wound edges by TGF-β1 (1–4). Collectively, these suggest that periostin deposition and the formation of fibroblast-enriched granulation tissues is the critical step during wound repair. The significance of fibroblast activation during wound repair is also supported by data from profibrotic cytokine, FGF2-null mice (41). Therefore, it is likely that direct or indirect activation of dermal fibroblasts by presence of periostin may be an additional mechanism underlying

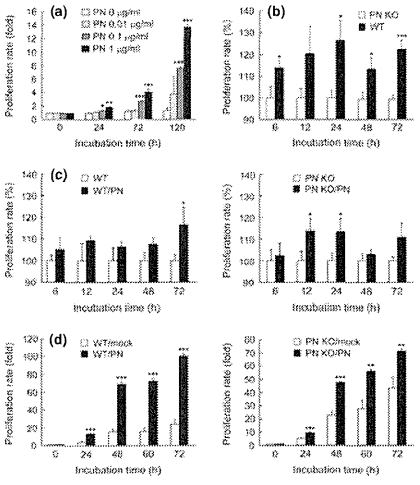

Figure 3. Effects of periostin on fibroblast proliferation. (a–c) Normal human dermal fibroblasts (a) or mouse dermal fibroblasts derived from wild-type (WT) or periostin-deficient mice (PN KO) (b, c) were cultured for various times. In panel (a), the concentrations of human periostin used are indicated, and in panel (c), 100 ng/ml of mouse periostin was used to coat the culture dishes. (d) Mouse periostin-overexpressed or mock-transduced MEFs (3×10^3 cells) derived from wild-type (WT) or periostin-deficient (PN KO) mice were cultured for various lengths. The proliferation rate was estimated using the Cell Counting Reagent SF. The relative folds were compared with the starting points (a, d) or PN KO-type or to fibroblasts on non-coated plates (b, c) are depicted. In panel (a), one-way ANOVA followed by Dunnett's test was used for multiple comparisons of the different fibroblast rates induced by various concentrations of periostin. Statistical differences were compared with PN 0 ng/ml cultures. Experiments were repeated five times, and the representative combined data are depicted. $^*P < 0.05$, $^{**}P < 0.01$, $^{***}P < 0.001$.

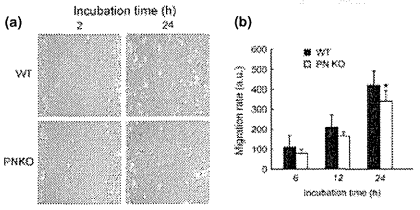

Figure 4. Effects of periostin on the migration of fibroblasts. Analysis of cell migration in MEFs derived from wild-type (WT) or periostin-deficient (PN KO) mice were compared. Photographs of the wounded cell monolayers at 2 and 24 h (a) and the relative cell motilities at various times indicated (b). The average cell motility (14 points per one field and three different fields/well in triplicate) was calculated and shown. Statistical difference between WT vs PN KO ($^*P < 0.05$) is depicted.

wound repair, in addition to periostin activation of keratinocytes (40).

It is well known that TGF-β1 is highly expressed in wounded tissues and can act as a central enhancer of wound repair effectors (42,43). Consequently, mice deficient in TGF-β1 show delayed cutaneous wound repair (44). When we examined whether TGF-β1 or other cytokines were able to directly induce periostin expression in human dermal fibroblasts and accumulated periostin in the supernatant was seen in responses to IL-4 and IL-13 (17,18) and to TGF-β1, whereas several other cytokines (IL-1β, -6, -17, tumor necrosis factor-α, FGF-2, FGF-5, stromal cell-derived factor-1, and PDGF) were not able to induce periostin expression (Fig. S9). Collectively, these results suggest that TGF-β1, abundant in the wound site, mainly contributes to periostin induction and that induction of periostin is a novel biological function of TGF-β1 within the well-ordered process of wound repair.

Targeted genetic deletion of periostin in mice significantly impairs fibroblast proliferation and wound healing, whereas fibroblast proliferation and wound healing can be enhanced by exogenous periostin, suggesting a direct role for periostin. Furthermore, treatment of dermal fibroblasts with exogenous periostin activates integrin-associated signalling molecules (FAK, STAT3, Akt and p44/42MAPK). As integrin-mediated signalling is initiated by formation of the Src/FAK complex, which enhances cell proliferation by up-regulating cyclin D1 expression via p44/42MAPK or cell survival by inhibiting proapoptotic factors such as Bad, caspase nine, forkhead transcription factors via PI3K/Akt (10–12), our results indicate that several levels of the proliferation pathway are activated when periostin is present. Moreover, STAT3 transduces signals important for cell proliferation and survival, cooperating with growth factor receptor-mediated signals (45,46). Periostin has been shown to induce proliferation of smooth muscle and/or cancer cells via the FAK/PI3K/Akt pathway (47,48). In contrast, genetic inhibition or administration of MAPK inhibitors delays wound repair (49,50). Finally, direct activation of the PI3K/Akt pathway is known to accelerate wound repair (51). These collective results suggest that periostin–integrins signal via FAK, STAT3, Akt and p44/42MAPK and play an important role in wound repair via augmenting cell proliferation/survival.

Clinically, it may be imperative to modulate either delayed (e.g. from diabetes or radiation exposure) or enhanced wound repair [e.g. hypertrophic and keloid scars (2,3)]. However, disappointing clinical results from single-agent therapies such as administering growth factors or other mediators to boost wound repair suggest that it is a highly ordered and complex process. Our surprising result, that injection of periostin into the wound in mice models can accelerate the healing process, may suggest that topical administration of periostin could be efficacious in wound treatment. Furthermore, it is now hoped that recent advances in stem cell/progenitor cell biology and material sciences will make it possible to entirely replace tissues. Our present data regarding the role of periostin in wound repair indicate that it could be a useful addition in construction of optimized skin tissues.

In conclusion, in this study, we demonstrate that periostin, transiently expressed during wound repair, accelerates the process by activating dermal fibroblasts. Although the pathological roles of periostin within fibrosis in various diseases have recently been well characterized, the physiological roles of periostin in skin repair are starting to be uncovered. Our present study demonstrates a novel physiological role for periostin: namely, its involvement in effective cutaneous wound repair.

Acknowledgements

We thank Dr. Dovie R. Wylie, Hiroyuki Ideguchi, Yumiko Ohishi, Yukako Kanazawa and Maiko Urase for critical review of this manuscript, technical and secretarial assistance. KO, YK, HS, SS and LY performed the research. AT, MF, YN, HM, ST, IK, KI and TN designed the research study. SO, KA, SS, AK and SJC contributed essential reagents or tools. KO, YK, SJC and KI wrote the paper. This work was supported in part by Grants-in-Aid for Scientific Research from the Japan Society for the Promotion of Science and by Grant-in-Aid from the Ministry of Health, Labour and Welfare, Japan.

Conflict of interests

The authors have no declared no conflicts of interests.

References

1 Baum C L, Arpey C J. Dermatol Surg 2005: **31**: 674–686.
2 Gurtner G C, Werner S, Barrandon Y *et al.* Nature 2008: **453**: 314–321.
3 Singer A J, Clark R A. N Engl J Med 1999: **341**: 738–746.
4 Palatinus J A, Rhett J M, Gourdie R G. J Mol Cell Cardiol 2010: **48**: 550–557.
5 Ranzato E, Martinotti S, Volante A *et al.* Exp Dermatol 2011: **20**: 308–313.
6 Kim J H, Jung M, Kim H S *et al.* Exp Dermatol 2011: **20**: 383–387.
7 Novotny M, Vasilenko T, Varinska L *et al.* Exp Dermatol 2011: **20**: 703–708.
8 Werner S, Grose R. Physiol Rev 2003: **83**: 835–870.
9 Desmouliere A, Geinoz A, Gabbiani F *et al.* J Cell Biol 1993: **122**: 103–111.
10 Eliceiri B P. Circ Res 2001: **89**: 1104–1110.
11 Giancotti F G, Ruoslahti E. Science 1999: **285**: 1028–1032.
12 Hynes R O. Trends Cell Biol 1999: **9**: M33–M37.
13 Hamilton D W. J Cell Commun Signal 2008: **2**: 9–17.
14 Rios H, Koushik S V, Wang H *et al.* Mol Cell Biol 2005: **25**: 11131–11144.
15 Midwood K, Sacre S, Piccinini A M *et al.* Nat Med 2009: **15**: 774–780.
16 Shinohara M L, Kim J H, Garcia V A *et al.* Immunity 2008: **29**: 68–78.
17 Hayashi N, Yoshimoto T, Izuhara K *et al.* Proc Natl Acad Sci U S A 2007: **104**: 14765–14770.
18 Takayama G, Arima K, Kanaji T *et al.* J Allergy Clin Immunol 2006: **118**: 98–104.
19 Woodruff P G, Boushey H A, Dolganov G M *et al.* Proc Natl Acad Sci U S A 2007: **104**: 15858–15863.
20 Okamoto M, Hoshino T, Kitasato Y *et al.* Eur Respir J 2011: **37**: 1119–1127.
21 Shimazaki M, Nakamura K, Kii I *et al.* J Exp Med 2008: **205**: 295–303.
22 Hakuno D, Kimura N, Yoshioka M *et al.* J Clin Invest 2010: **120**: 2292–2306.
23 Oku E, Kanaji T, Takata Y *et al.* Int J Hematol 2008: **88**: 57–63.
24 Yoshida S, Ishikawa K, Asato R *et al.* Invest Ophthalmol Vis Sci 2011: **52**: 5670–5678.
25 Blanchard C, Mingler M K, McBride M *et al.* Mucosal Immunol 2008: **1**: 289–296.
26 Sidhu S S, Yuan S, Innes A L *et al.* Proc Natl Acad Sci U S A 2010: **107**: 14170–14175.
27 Kuhn B, del Monte F, Hajjar R J *et al.* Nat Med 2007: **13**: 962–969.
28 Lorts A, Schwanekamp J A, Elrod J W *et al.* Circ Res 2009: **104**: e1–e7.
29 Fujimoto K, Kawaguchi T, Nakashima O *et al.* Oncol Rep 2011: **25**: 1211–1216.
30 Ruan K, Bao S, Ouyang G. Cell Mol Life Sci 2009: **66**: 2219–2230.
31 Snider P, Hinton R B, Moreno-Rodriguez R A *et al.* Circ Res 2008: **102**: 752–760.
32 Jackson-Boeters L, Wen W, Hamilton D W. J Cell Commun Signal 2009: **3**: 125–133.
33 Zhou H M, Wang J, Elliott C *et al.* J Cell Commun Signal 2010: **4**: 99–107.
34 Kitamura T, Koshino Y, Shibata F *et al.* Exp Hematol 2003: **31**: 1007–1014.
35 Midwood K S, Williams L V, Schwarzbauer J E. Int J Biochem Cell Biol 2004: **36**: 1031–1037.
36 Echtermeyer F, Streit M, Wilcox-Adelman S *et al.* J Clin Invest 2001: **107**: R9–R14.
37 Muro A F, Chauhan A K, Gajovic S *et al.* J Cell Biol 2003: **162**: 149–160.
38 Kyriakides T R, Tam J W, Bornstein P. J Invest Dermatol 1999: **113**: 782–787.
39 Streit M, Velasco P, Riccardi L *et al.* EMBO J 2000: **19**: 3272–3282.
40 Nishiyama T, Kii I, Kashima T G *et al.* PLoS One 2011: **6**: e18410.
41 Ortega S, Ittmann M, Tsang S H *et al.* Proc Natl Acad Sci U S A 1998: **95**: 5672–5677.
42 Barrientos S, Stojadinovic O, Golinko M S *et al.* Wound Repair Regen 2008: **16**: 585–601.
43 Werner S, Krieg T, Smola H. J Invest Dermatol 2007: **127**: 998–1008.
44 Crowe M J, Doetschman T, Greenhalgh D G. J Invest Dermatol 2000: **115**: 3–11.
45 Guo W, Pylayeva Y, Pepe A *et al.* Cell 2006: **126**: 489–502.
46 Shin H D, Park B L, Kim L H *et al.* Hum Mol Genet 2004: **13**: 397–403.
47 Bao S, Ouyang G, Bai X *et al.* Cancer Cell 2004: **5**: 329–339.
48 Li G, Jin R, Norris R A *et al.* Atherosclerosis 2010: **208**: 358–365.
49 Sharma G D, He J, Bazan H E. J Biol Chem 2003: **278**: 21989–21997.
50 Thuraisingam T, Xu Y Z, Eadie K *et al.* J Invest Dermatol 2010: **130**: 278–286.
51 Lai J P, Dalton J T, Knoell D L. Br J Pharmacol 2007: **152**: 1172–1184.

Supporting Information

Additional Supporting Information may be found in the online version of this article:

Figure S1. Periostin expression in wounded tissues.
Figure S2. Expression of periostin in the wound sites in mice.
Figure S3. Periostin is important for efficient wound healing in mice.
Figure S4. Periostin is important for efficient wound healing in mice.
Figure S5. Activation of human dermal fibroblasts by exogenous periostin.
Figure S6. Effects of fibroblast growth factor-2 on fibroblast proliferation.
Figure S7. Establishment of periostin-transduced MEFs.
Figure S8. Effects of cytochalasin D and platelet-derived growth factor on cell migration.
Figure S9. Analysis of periostin responses in human dermal fibroblasts to various stimuli.
Data S1. Materials and methods.

Please note: Wiley-Blackwell is not responsible for the content or functionality of any supporting materials supplied by the authors. Any queries (other than missing material) should be directed to the corresponding author for the article.

Serum Leucine-rich Alpha-2 Glycoprotein Is a Disease Activity Biomarker in Ulcerative Colitis

Satoshi Serada, PhD, Minoru Fujimoto, MD, PhD,* Fumitaka Terabe, MD, PhD,*† Hideki Iijima, MD, PhD,† Shinichiro Shinzaki, MD, PhD,† Shinya Matsuzaki, MD,‡ Tomoharu Ohkawara, MD,* Riichiro Nezu, MD, PhD,§ Sachiko Nakajima, MD, PhD,† Taku Kobayashi, MD, PhD,‖ Scott Eric Plevy, MD, PhD,‖ Tetsuo Takehara, MD, PhD,† and Tetsuji Naka, MD, PhD**

Background: Reliable biomarkers for monitoring disease activity have not been clinically established in ulcerative colitis (UC). This study aimed to investigate whether levels of serum leucine-rich alpha-2 glycoprotein (LRG), identified recently as a potential disease activity marker in Crohn's disease and rheumatoid arthritis, correlate with disease activity in UC.

Methods: Serum LRG concentrations were determined by enzyme-linked immunosorbent assay (ELISA) in patients with UC and healthy controls (HC) and were evaluated for correlation with disease activity. Expression of LRG in inflamed colonic tissues from patients with UC was analyzed by western blotting and immunohistochemistry. Interleukin (IL)-6-independent induction of LRG was investigated using IL-6-deficient mice by lipopolysaccharide (LPS)-mediated acute inflammation and dextran sodium sulfate (DSS)-induced colitis.

Results: Serum LRG concentrations were significantly elevated in active UC patients compared with patients in remission ($P < 0.0001$) and HC ($P < 0.0001$) and were correlated with disease activity in UC better than C-reactive protein (CRP). Expression of LRG was increased in inflamed colonic tissues in UC. Tumor necrosis factor alpha (TNF-α), IL-6, and IL-22, serum levels of which were elevated in patients with active UC, could induce LRG expression in COLO205 cells. Serum LRG levels were increased in IL-6-deficient mice with LPS-mediated acute inflammation and DSS-induced colitis.

Conclusions: Serum LRG concentrations correlate well with disease activity in UC. LRG induction is robust in inflamed colons and is likely to involve an IL-6-independent pathway. Serum LRG is thus a novel serum biomarker for monitoring disease activity in UC and is a promising surrogate for CRP.

(Inflamm Bowel Dis 2012;000:000–000)

Key Words: IBD, ulcerative colitis, biomarker, leucine-rich alpha-2 glycoprotein, DSS

The chronic inflammatory bowel diseases (IBDs), Crohn's disease (CD) and ulcerative colitis (UC), are typically characterized by episodes of acute flares and remission.[1,2] Depending on disease location and extent, exacerbation leads to diarrhea, abdominal pain, and systemic symptoms such as fatigue and weight loss.[3–5] Disease activity indices have been developed as outcome measures in clinical trials.[6,7] They may help to reproducibly and validly assess the patients' status and to support therapeutic decision-making.[6] Variables of disease activity indices comprise frequency of bowel movements, severity of abdominal pain, general well-being, occurrence of extraintestinal manifestations, and laboratory parameters.[8]

One of the most important protein biomarkers increased during the inflammatory state is C-reactive protein (CRP). However, elevation of serum CRP levels is not observed in certain inflammatory diseases. While serum CRP levels are highly increased in CD and rheumatoid arthritis (RA) patients and widely used for monitoring disease activity, only modest to absent CRP responses are observed in systemic lupus erythematosus (SLE), dermatomyositis, Sjogren's syndrome, or UC, although active inflammation is present.[9–11] In UC, endoscopic disease activity may predict future clinical symptoms,[12] but direct endoscopic or radiologic visualization of the degree of inflammation is rarely performed in outpatients with inactive or mild disease. Therefore, alternative biomarkers, which can conveniently and precisely monitor disease activity during therapy in inflammatory diseases, are required for the determination of adequate treatment.

By using a quantitative proteomic approach, we have previously reported that serum levels of leucine-rich alpha-2 glycoprotein (LRG) were elevated in patients with active RA and serum LRG levels were correlated with disease activity of not only RA but also CD, suggesting that serum LRG is a serological biomarker for monitoring disease activity.[13] LRG is an ≈50 kDa glycoprotein and contains repetitive sequences with a leucine-rich motif, first purified from human serum.[14,15] LRG has been reported to be expressed by the liver cells and neutrophils[16,17]; however, its function remains unclear. To date, the relationship between serum LRG levels and disease activity in UC has not been assessed. In this study we investigated serum LRG expression levels in UC patients and evaluated their correlation with clinical disease activity. Serum LRG levels were significantly increased in the active UC patients. LRG expression was upregulated in the inflamed colonic mucosa of UC possibly through stimulation by various cytokines including tumor necrosis factor alpha (TNF-α), interleukin (IL)-6, and IL-22, the expression of which are increased in active UC. Moreover, we show that serum LRG correlates more strongly than CRP with disease activity in UC. Therefore, serum LRG may be a useful disease activity biomarker for UC.

Additional Supporting Information may be found in the online version of this article.

Received for publication February 12, 2012; Accepted February 13, 2012.

From the *Laboratory for Immune Signal, National Institute of Biomedical Innovation, Osaka, Japan, †Department of Gastroenterology and Hepatology, Osaka University Graduate School of Medicine, Osaka, Japan, ‡Department of Obstetrics and Gynecology, Osaka University Graduate School of Medicine, Osaka, Japan, §Department of Surgery, Osaka Rosai Hospital, Osaka, Japan, ‖Center for Gastrointestinal Biology and Diseases, University of North Carolina School of Medicine, Chapel Hill, North Carolina, USA.

Supported by the Grant-in-Aid for Scientific Research (C) (22591101) from the Japanese Ministry of Education, Science, Sports, and Culture; a grant-in-aid for the Program for Promotion of Fundamental Studies in Health Sciences of the National Institute of Biomedical Innovation and Grant-in-Aid from the Ministry of Health, Labour and Welfare of Japan.

Reprints: Tetsuji Naka, Laboratory for Immune Signal, National Institute of Biomedical Innovation, 7-6-8, Saito-asagi, Ibaraki, Osaka 567-0085, Japan (e-mail: tnaka@nibio.go.jp).

DOI 10.1002/ibd.22936

Published online in Wiley Online Library (wileyonlinelibrary.com).

TABLE 1. Characteristics of Patients with Ulcerative Colitis (UC)

Characteristics	Patients with UC	Patients with Appendicitis and Diverticulitis
Number (male:female)	82 (41:41)	17 (8:9)
Age, yr, mean (SD)	40.1 (15.7)	33.1 (13.7)
Age at diagnosis, yr, mean (SD)	34.7 (15.6)	33.1 (13.7)
Bowel surgery (including appendectomy), *N* (%)	7 (8.54)	
Treatment		
Salazosulfapyridine or mesalazine, N (%)	66 (80.5)	
Steroids, *N* (%)	16 (19.5)	
Immunomodulators, N (%)	3 (3.7)	
Disease location (*N*)		
Extensive colitis/left-sided colitis/proctitis	37/30/15	
CRP, mg/dL, mean (SD)	0.884 (1.967)	8.47 (7.69)
WBC cells/μl, mean (SD)	6716 (2317)	12307 (3603)
CAI, mean (SD)	4.71 (4.89)	
Matts's score, mean (SD)	2.27 (0.89)	

MATERIALS AND METHODS

Patients and Sera

Sera were obtained from patients with UC ($n = 82$), appendicitis ($n = 13$), and diverticulitis ($n = 4$) and surgical or biopsy samples were obtained from patients with UC ($n = 10$) from Osaka University Hospital (Osaka, Japan) and the Department of Surgery, Osaka Rosai Hospital, respectively. Sera from healthy controls (HCs) ($n = 50$), age/sex-matched with UC patients, were used. Diagnosis of UC was based on conventional clinical, radiological, endoscopic, and histopathological criteria. Clinical activities were determined using the Clinical Activity Index (CAI) for UC.[18] Clinical remission was defined as CAI <6.[19] In addition to CAI, the endoscopic findings were also graded according to Matts' criteria.[20] Endoscopic remission was defined as Matts' score ≤2. Detailed patient characteristics are presented in Table 1. For Caucasian patients with UC, sera ($n = 30$) were obtained from the Department of Medicine, University of North Carolina Hospital (Chapel Hill, NC). Sera from HCs ($n = 19$), age/sex-matched with UC patients, were used. Detailed patient characteristics are presented in Table 2, while data of disease activity of UC is not available.

Quantification of Serum LRG and Cytokines

Human serum LRG and mouse serum LRG were quantitated by human LRG assay kit (IBL, Fujioka, Japan) and mouse LRG assay kit (IBL, Fujioka, Japan). These enzyme-linked immunosorbent assay (ELISA) assays were performed

TABLE 2. Characteristics of Patients with UC in a Caucasian Cohort

Characteristics	Patients with UC
Number (male:female)	30 (18:12)
Age, yr, mean (SD)	42.9 (17.9)
Age at diagnosis, yr, mean (SD)	33.2 (15.7)
Treatment	
Salazosulfapyridine or mesalazine, *N* (%)	14 (46.7)
Steroids, *N* (%)	9 (30.0)
Immunomodulators, *N* (%)	11 (36.7)
Anti-TNF therapy	3 (10.0)
Disease location (*N*)	
Extensive colitis/left-sided colitis/proctitis	16/11/3

in duplicate. The intraassay coefficients of variations for human LRG and mouse LRG were ≤7.98% and ≤8.93%, respectively. For the quantification of IL-6, TNF-α, and IL-22 in human serum samples, the human IL-6 Ultra Sensitive ELISA (Biosource International, Camarillo, CA), human TNF-α UltraSensitive ELISA kit (Invitrogen, Carlsbad, CA), and human IL-22 Quantikine ELISA Kit (R&D Systems, Minneapolis, MN) were used following the manufacturer's guidelines.

Western Blot Analysis

Frozen colon tissue samples were lysed in RIPA buffer (10 mM Tris-HCl, pH 7.5, 150 mM NaCl, 1% Nonidet P-40, 0.1% sodium deoxycholate, 0.1% SDS, 1 × protease inhibitor cocktail; Nacalai Tesque, Kyoto, Japan) and 1 × phosphatase inhibitor cocktail (Nacalai Tesque) followed by centrifugation (13,200 rpm, 4°C, 15 minutes), after which the supernatants were stored at −80°C until use. Extracted proteins were subjected to sodium dodecyl sulfate-polyacrylamide gel electrophoresis (SDS-PAGE) as described previously.[21] Samples transferred onto PVDF membranes were treated with a rabbit antihuman LRG polyclonal antibody (Proteintech Group, Chicago, IL) or a rabbit anti-GAPDH polyclonal antibody (Santa Cruz Biotechnology, Santa Cruz, CA) was used as described previously.[21]

Immunohistochemistry

Immunohistochemical analyses were performed according to a method described in our previous report.[22] Briefly, rabbit antihuman LRG polyclonal antibodies were used as the primary antibody. After incubation with the primary antibodies, the sections were treated with biotin-conjugated goat anti-rabbit IgG (Vector Laboratories, Burlingame, CA) and avidin-biotin-peroxidase complexes (Vector Laboratories). Immunoreactive cells were visualized with a diaminobenzidine substrate (Merck, Darmstadt, Germany) and were counterstained with hematoxylin.

Mice

C57BL/6 mice were purchased from Clea Japan (Tokyo, Japan). C57BL/6-background IL-6-deficient mice were kindly provided by Professor Yoichiro Iwakura (Laboratory of Molecular Pathogenesis, Center for Experimental Medicine, Institute of Medical Science, University of Tokyo, Tokyo, Japan). Mice were maintained under specific pathogen-free conditions. C57BL/6 and IL-6-deficient mice were used at 7–9 weeks of age. All experiments were conducted according to the institutional ethical guidelines for animal experimentation.

LPS-mediated Acute Inflammation

To induce acute inflammation, wildtype (WT) mice and IL-6-deficient mice were injected intraperitoneally with 0 or 10 mg/kg LPS (*Escherichia coli* LPS, Sigma, St. Louis, MO) dissolved in 500 μL phosphate-buffered saline (PBS). Blood was collected at before and 24 hours after LPS injection and the serum was separated by centrifugation and stored at −30°C until used for ELISA analysis.

Induction of Colitis

For induction of colitis, WT mice and IL-6-deficient mice were given 3% dextran sodium sulfate (DSS) (m/w 36,000–50,000; MP Biomedicals, Solon, OH) dissolved in drinking water provided ad libitum for 5 days, followed by provision of ordinary water for 20 days.

Assessment of Severity of DSS-induced Colitis

WT mice were weighed daily from day 0 to day 25. Changes in body weight were calculated as follows: body weight change (%) = [(weight on a given day (days 0–13) − weight on day 0)/weight on day 0] * 100. Blood was collected from WT mice on days 5, 7, 10, 15, and 25 after DSS administration or day 0 by cardiac puncture under anesthesia and on days 0 and 10 from IL-6-deficient mice. The serum was separated by centrifugation and stored at −30°C until used for ELISA analysis.

Cell Culture

The human colonic adenocarcinoma COLO205 cell line was obtained from the American Type Culture Collection (ATCC, Manassas, VA). Cells were maintained in RPMI 1640 medium supplemented with 10% fetal bovine serum (FBS) (HyClone Laboratories, Logan, UT) and 1% penicillin–streptomycin (Nacalai Tesque) at 37°C under a humidified atmosphere of 5% CO_2.

For the analysis of LRG protein induction, COLO205 cells were stimulated with various concentrations of cytokines for 24 hours and culture supernatant were concentrated using Amicon Ultra-4 10K MWCO (Millipore, Bedford, MA). Concentrated supernatants were used for western blot analysis. Full-length human LRG cDNA was inserted into pcDNA3.1/V5-His-TOPO vector (Invitrogen) and designated pcDNA3.1-LRG-V5-His. pcDNA3.1-LRG-V5-His vector was transfected

into COS7 cells using Lipofectamine 2000 reagent (Invitrogen) and culture medium were used for the positive control.

Quantitative Real-time Reverse-transcription Polymerase Chain Reaction (RT-PCR) Analysis

For the quantification of mRNA levels of LRG, various mouse organs were analyzed by real-time RT-PCR as described previously.[23] Levels of mouse LRG and mouse hypoxanthine phosphoribosyltransferase (HPRT) levels were determined by the 7900HT Real-time PCR system (Applied Biosystems, Foster City, CA) using specific primers: murine LRG forward 5′-ATCAAGGAAGCCTCCAGGAT-3′; reverse 5′-CAGCTGCGTCAGGTTGG-3′ and murine hypoxanitine phosphoribosyltransferase (HPRT) forward 5′-TCAGTCAACG GGGGACATAAA-3′; reverse 5′-GGGGCTGTACTGCTT AACCAG-3′.

Statistics

The Mann–Whitney *U*-test or one-way analysis of variance (ANOVA) followed by a Scheffe's test were used for statistical analyses. Two-tailed Student's *t*-test was used for significant differences in LRG expression between identical patients with UC in active and remission disease stage. One-way ANOVA followed by a Dunnett's test was used for multiple comparison of the difference of serum LRG levels at various timepoints after DSS treatment in mice. Pearson's test was used to analyze the relationship between LRG and CRP, IL-6, or CAI. For drawing of receiver operating characteristic (ROC) curves and estimation of the area under the ROC curve (AUC) statistics, the software Excel Statistics 2010 (Social Survey Research Information, Tokyo, Japan) was used to quantify the ability to differentiate between remission and active by CAI. $P < 0.05$ was considered significant.

Ethical Considerations

Informed consent was obtained from all donors and all studies involving human subjects were approved by the Institutional Review Boards of the National Institute of Biomedical Innovation, Osaka University Hospital, the Department of Surgery, Osaka Rosai Hospital, and the University of North Carolina.

RESULTS

Serum LRG Levels Are Increased in Active UC Patients

We quantified serum LRG concentrations by ELISA using sera from patients with UC. Serum LRG concentrations were significantly elevated in the active UC patients (CAI ≥6) (14.24 ± 8.08 μg/mL) compared with HC (3.07 ± 1.42 μg/mL; $P < 0.0001$) (Fig. 1A). There was also a significant difference between LRG serum levels in patients with active UC (CAI ≥6) (14.24 ± 8.08 μg/mL) compared with UC in remission (CAI <6) (5.34 ± 2.60 μg/mL; $P <$

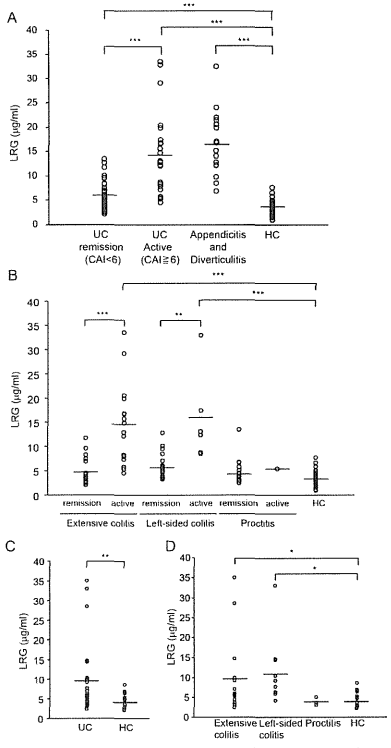

FIGURE 1. Serum LRG levels are increased in patients with active UC. (A) Serum levels of LRG were determined in 82 patients with UC (57 patients in remission [CAI <6], 25 patients in active [CAI ≥6] stage), appendicitis ($n = 13$), diverticulitis ($n = 4$) and 50 healthy controls (HC). ***$P < 0.0001$ by one-way ANOVA followed by Scheffe's post-hoc test. (B) Disease extension in UC was grouped into three categories: In UC patients in remission, extensive colitis ($n = 19$), left-sided colitis ($n = 24$), and proctitis ($n = 14$); in active patients, extensive colitis ($n = 18$), left-sided colitis ($n = 6$), and proctitis ($n = 1$) and HC ($n = 50$). **$P < 0.005$, ***$P < 0.0001$ by one-way ANOVA followed by Scheffe's post-hoc test. (C) Serum levels of LRG were determined in patients with UC ($n = 30$) and HC ($n = 19$) in a Caucasian cohort. **$P < 0.005$ by Mann–Whitney *U*-test. (D) In a Caucasian cohort, disease extension in UC was grouped into three categories: extensive colitis ($n = 16$), left-sided colitis ($n = 11$), and proctitis ($n = 3$) and HC ($n = 19$). *$P < 0.05$ by one-way ANOVA followed by Scheffe's post-hoc test.

0.0001) (Fig. 1A). To determine whether serum LRG levels are increased in non-IBD disease controls, we quantified serum LRG levels in patients with appendicitis and

diverticulitis. Elevated serum LRG levels were also observed in appendicitis and diverticulitis (16.83 ± 6.50 μg/mL) compared with HC (3.07 ± 1.42 μg/mL; $P < 0.0001$) (Fig. 1A), suggesting that serum LRG levels are also increased in acute intestinal inflammation.

When UC were classified into three categories based on disease extent, significantly higher serum LRG concentrations were observed in active patients with extensive colitis (14.34 ± 7.89 μg/mL) compared with in remission (4.96 ± 2.68 μg/mL; $P < 0.0001$) and HC (3.07 ±1.42 μg/mL; $P < 0.0001$) and active patients with left-sided colitis (15.41 ± 9.16 μg/mL) compared with in remission (5.91 ± 2.41 μg/mL; $P = 0.0003$) and HC (3.07 ±1.42 μg/mL; $P = 0.001$) (Fig. 1B). Nonetheless, there was no clear difference between active patients with proctitis and HC, possibly due to the low number of patients in this group. In patients with UC in remission, serum LRG levels in all of three disease extent categories were comparable with HC (Fig. 1B). Significantly elevated serum LRG levels were also detected in a Caucasian UC cohort (9.46 ± 8.44 μg/mL) compared with HC (4.42 ± 1.91 μg/mL; $P < 0.005$) (Fig. 1C). In this Caucasian UC cohort, serum LRG levels were also significantly elevated in patients with extensive colitis (9.54 ± 8.05 μg/mL) compared with HC (4.42 ± 1.91 μg/mL; $P < 0.05$) and left-sided colitis (10.90 ± 9.16 μg/mL) compared with HC (4.42 ± 1.91 μg/mL; $P < 0.02$) (Fig. 1D). However, a clear difference was not observed between patients with proctitis and HC (Fig. 1D). These results suggest that serum LRG levels were elevated in active UC.

Serum LRG Levels Are Correlated with Disease Activity in UC Patients

We investigated the correlation between serum LRG levels and disease activity (CAI) in UC patients. A positive correlation was observed between LRG and CAI ($r = 0.731$, $P < 0.00001$) (Fig. 2A). This correlation was stronger than that observed between CRP and CAI ($r = 0.654$, $P < 0.00001$) (Fig. 2A). When patients with UC were classified into active and remission according to the endoscopic findings, significantly elevated serum LRG levels and CRP levels were observed in patients with active UC compared with patients in remission ($P < 0.005$, respectively) (Supporting Fig. 1A). While serum LRG levels were significantly correlated with CRP levels in patients with UC ($r = 0.850$, $P < 0.00001$, $n = 82$) (Supporting Fig. 2A), such a correlation was not found when a CRP-negative subgroup (CRP <0.2, $n = 51$) was analyzed ($r = 0.101$, $P = 0.481$) (Supporting Fig. 2B). In this CRP-negative group, serum LRG levels were significantly correlated with CAI ($r = 0.416$, $P = 0.00241$) (Supporting Fig. 2C); however, significant correlation was not found between CRP and CAI ($r = -0.0896$, $P = 0.532$) (Supporting Fig. 2D). Additionally, in the CRP-negative group elevated serum LRG levels were detected in patients with endoscopically active UC compared with patients with UC in remission ($P = 0.0442$) (Supporting Fig. 1B). These findings in patients with low CRP may explain a better correlation of CAI with LRG than that with CRP.

When UC was classified by disease extent, a significantly higher positive correlation was detected between LRG and CAI than CRP and CAI both in extensive colitis ($r = 0.690$, $P < 0.000001$ and $r = 0.580$, $P = 0.000168$) and left-sided colitis ($r = 0.840$, $P < 0.000001$ and $r = 0.759$, $P < 0.000001$), but not in proctitis (Fig. 2B). Importantly, by analyzing sera obtained at active (CAI ≥6) and remission (CAI <6) disease stages from 10 identical UC patients, a significant decrease in serum LRG levels in remission was detected (Fig. 2C).

By generating an ROC curve, the sensitivity and specificity of serum LRG for remission and active by CAI were determined (Fig. 2D). The AUC for serum LRG levels was 0.901, whereas the AUC for CRP levels was 0.845. The cutoff value of serum LRG levels was 7.21 μg/mL (sensitivity = 84.0%, specificity = 82.5%). In contrast, when the cutoff value of CRP levels was set to 0.20, a maximum CRP value of normal range, the sensitivity was 80.0% and the specificity was 80.7%. These results emphasize the usefulness of monitoring serum LRG levels for the evaluation of the disease activity of UC.

Expression of LRG Was Increased in Inflamed UC Colons

Next, to investigate whether local inflammatory sites in patients with UC are a potential source of increased serum LRG we first looked at the expression of LRG in the colon by western blot analysis on inflamed and noninflamed sites of surgically resected full-thickness colon specimens from patients with UC. Western blot analysis showed that LRG expression in colon tissues was increased in inflamed sites of active UC patients compared with noninflamed colon tissues (Fig. 3A). Next, we tried to examine the localization of LRG. By immunohistochemistry, increased expression of LRG was detected in the cytoplasm of intestinal epithelial cells (IECs) in inflamed tissues (Fig. 3B–E). In contrast, expression of LRG was lower in noninflamed tissues (Fig. 3B–E). These data suggest that inflamed colon tissue is a potential source of increased serum LRG in patients with UC.

LRG Is Induced by Stimulation with TNF-α, IL-6, or IL-22

It has been reported that IL-6 is an inducer of LRG expression.[16] However, it is not clear whether LRG is induced by cytokines other than IL-6. At first we investigated the serum levels of IL-6, IL-22, and TNF-α, known

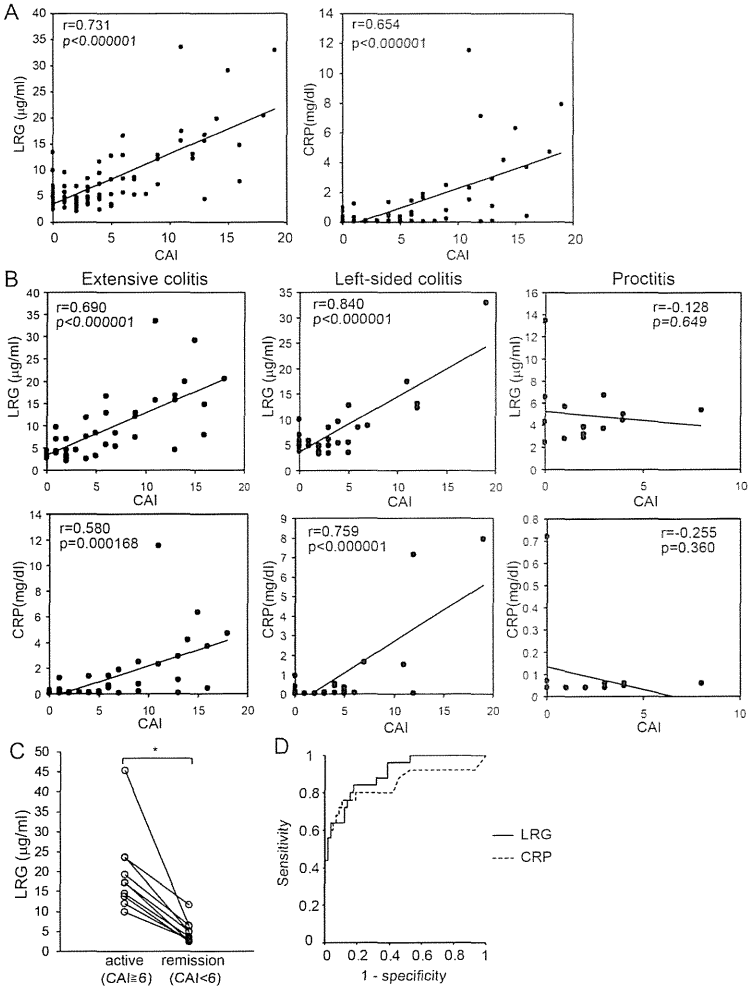

FIGURE 2. Serum LRG levels are correlated with disease activity better than CRP in patients with UC. (A) Serum levels of LRG correlated with CAI ($n = 82$; $P < 0.000001$; $r = 0.731$) better than CRP ($n = 82$; $P < 0.000001$; $r = 0.654$) in patients with UC. (B) Serum levels of LRG correlated with disease activity in extensive colitis ($n = 37$; $P < 0.000001$; $r = 0.690$) and left-sided colitis ($n = 30$; $P < 0.000001$; $r = 0.840$) better than CRP in extensive colitis ($n = 37$; $P = 0.000168$; $r = 0.580$) and left-sided colitis ($n = 30$; $P < 0.000001$; $r = 0.759$), while neither LRG ($n = 15$; $P = 0.649$; $r = -0.128$) nor CRP levels ($n = 15$; $P = 0.360$; $r = -0.255$) were correlated with disease activity in proctitis. (C) Compared with 10 identical active patients with UC, serum levels of LRG were decreased in remission. *$P < 0.002$ by Student's t-test. (D) ROC curves for LRG and CRP for differentiation between UC patients with remission ($n = 57$) and active ($n = 25$) by CAI.

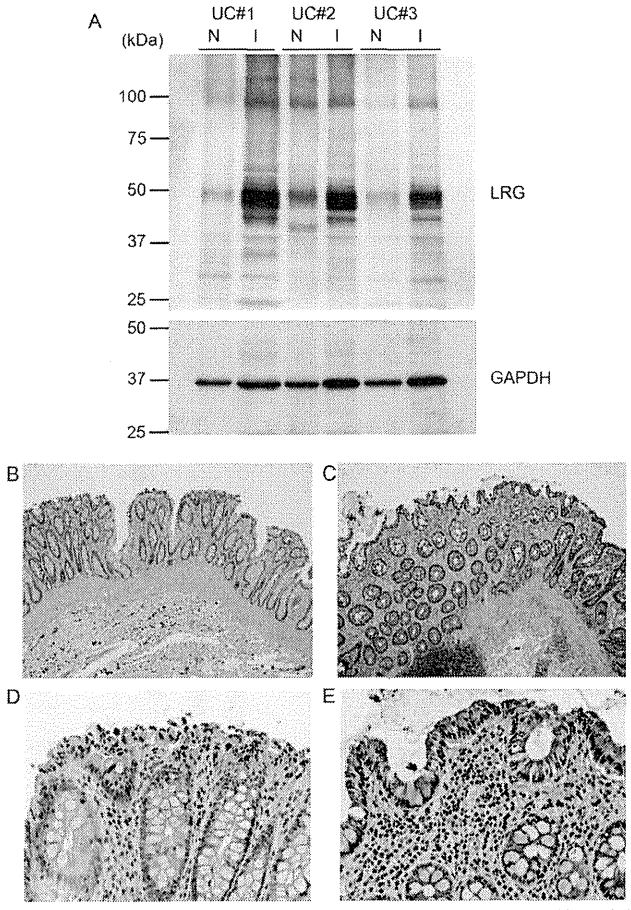

FIGURE 3. Expression of LRG is increased in lesion sites of ulcerative colitis. (A) Representative western blot analysis of three separate experiments for LRG using paired surgically resected full-thickness colon specimens from noninflamed (N) and inflamed (I) sites in patients with UC. GAPDH was used as a control of the relative amounts of proteins in each sample. Full-thickness colon tissues from UC in inflamed and noninflamed sites were evaluated by immunohistochemical analysis for LRG expression ($n = 10$ per experimental group). (B) Noninflamed mucosa (×42). (C) Inflamed mucosa from active UC (×42). (D) Noninflamed mucosa (×400). (E) Inflamed mucosa from active UC (×400).

to be increased at the inflamed tissue in active UC.[24–26] Indeed, ELISA analysis using sera from 82 UC patients revealed that serum TNF-α, IL-6, and IL-22 levels were significantly elevated in active UC patients compared with those patients in remission ($P = 0.0178$, $P = 0.00690$, and $P < 0.0001$, respectively) (Fig. 4A). Next, to investigate

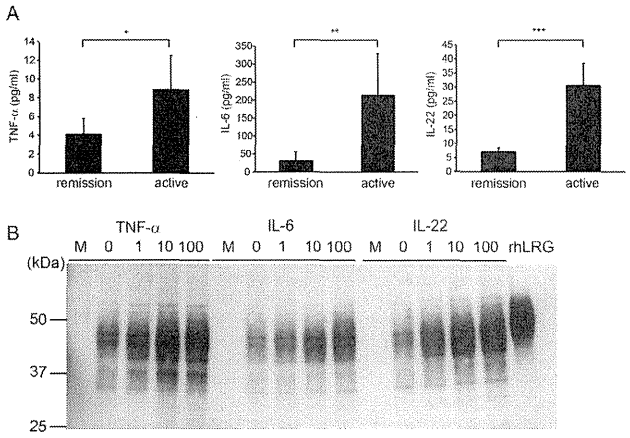

FIGURE 4. Expression of LRG was induced by TNF-α, IL-6, and IL-22. (A) Serum levels of TNF-α, IL-6, and IL-22 were determined in patients with UC (57 patients in remission [CAI <6] and 25 patients in active [CAI ≥6] stage). Data are expressed as mean ± SEM. *$P < 0.05$, **$P < 0.005$, ***$P < 0.0001$ by Mann–Whitney U-test. (B) LRG was determined in supernatants of COLO205 cells left untreated or stimulated with TNF-α, IL-6, and IL-22 at 1.0, 10, 100 ng/mL for 24 hours and analyzed by western blotting. There was a dose-dependent increase in LRG levels after treatment with TNF-α, IL-6, and IL-22.

which proinflammatory cytokines induce expression of LRG we stimulated human colonic adenocarcinoma COLO205 cells with TNF-α, IL-6, or IL-22 for 24 hours. After cytokine stimulation, secretion of LRG protein into the culture media was analyzed by western blotting. Interestingly, LRG was induced not only by stimulation with IL-6, but also by TNF-α and IL-22 in a dose-dependent manner (Fig. 4B). These results indicate that expression of LRG is induced by various proinflammatory cytokines including IL-6.

Expression of LRG Through an IL-6-independent Pathway Is Demonstrated in LPS-mediated Acute Inflammation and DSS-induced Colitis

CRP is one of the representative acute phase proteins in humans and CRP production is primarily dependent on liver by circulating IL-6. To examine the possible differences in induction mechanisms between LRG and CRP, particularly with regard to the involvement of IL-6, we took advantage of murine models. We first assessed whether LRG is induced in WT mice by injecting LPS, an inducer of proinflammatory cytokines from macrophages, because CRP is poorly induced in mice during acute inflammation. At 24 hours after intraperitoneal injection of LPS, serum samples were prepared and serum LRG levels were determined by ELISA. Compared with WT mice, significant elevation of serum LRG levels were detected in LPS-administered WT mice (Fig. 5A), suggesting that LRG is induced during acute inflammation in mice as in humans.

We next used a murine IBD model to investigate induction mechanisms of LRG during colonic inflammation. DSS-induced colitis is often used as a murine model of UC.[27] We induced colitis in WT mice by treating them with 3% DSS for 5 days and measured changes in relative body weight. Body weight began to decrease at day 5, showed greatest reduction at day 9, and recovered at 18 days after DSS treatment (Fig. 5B). We analyzed changes in serum LRG levels by ELISA before and 5, 7, 10, 15, and 25 days after DSS treatment. Consistent with body weight loss, serum LRG levels were significantly elevated at 5 days after DSS treatment (Fig. 5C). Serum LRG levels remained high until day 15, but decreased at day 25. Delayed normalization of serum LRG levels is likely due to the prolonged inflammation at inflamed tissue sites. Additionally, a long half-life of serum LRG might also be involved in this, since our preliminary data suggest that the half-life of serum human LRG levels are about two times longer than that of CRP (data not shown). To investigate which organs produce LRG in DSS-induced colitis, RNA was extracted from colon, liver, and spleen before and 9 days after DSS treatment. By quantitative PCR analysis (Fig. 5D), expression of LRG was significantly increased in liver ($P = 0.00106$) and spleen ($P = 0.0376$);

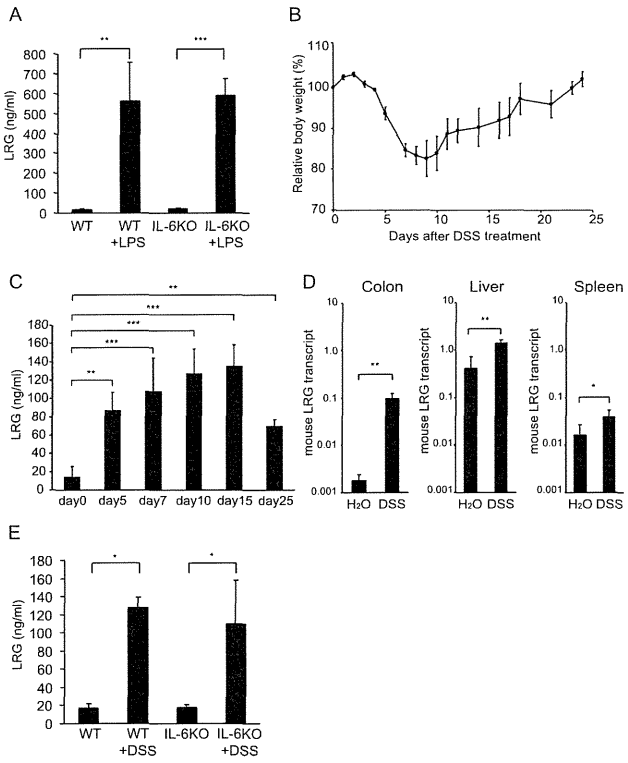

FIGURE 5. Induction of LRG has IL-6-independent pathway in LPS-mediated acute inflammation and active stage of DSS-induced colitis. (A) WT mice and IL-6-deficient mice were injected intraperitoneally with 0 or 10 mg/kg LPS dissolved in 500 μL PBS and serum LRG levels were measured after 24 hours. Data are expressed as mean ± SEM. $^{**}P < 0.005$, $^{***}P < 0.0001$ by one-way ANOVA followed by Scheffe's post-hoc test. (B) Relative body weight changes of mice with DSS-induced colitis in this study. Data are expressed as mean ± SEM ($n = 4$). (C) Expression of LRG is upregulated in murine DSS-induced colitis. At the indicated time, serum LRG levels were determined by ELISA analysis. $^{**}P < 0.005$, $^{***}P < 0.0001$ by one-way ANOVA followed by a by Dunnett's post-hoc test. (D) Nine days after control or DSS treatment, mice were euthanized and gene expression of LRG in the colon, liver, spleen, and kidney was determined by quantitative PCR analysis. Gene expression was calculated relative to HPRT. Data were expressed as mean ± SD ($n = 5$). $^{*}P < 0.05$, $^{**}P < 0.005$ by Student's t-test. (E) IL-6-deficient mice were used for DSS-induced colitis. Nine days after DSS administration, serum levels of mouse LRG was determined by ELISA analysis. $^{*}P < 0.05$ by one-way ANOVA followed by Scheffe's post-hoc test.

however, the strongest induction was observed in colon ($P = 0.000126$).

To investigate whether LRG induction is dependent on IL-6 or not, we analyzed serum LRG levels in IL-6-deficient mice. Interestingly, basal LRG levels in IL-6-deficient mice were similar to those in WT mice and LRG was robustly induced by LPS administration in IL-6-deficient mice (Fig. 5A). Moreover, increased serum LRG levels were also detected in the active stage (day 9) of DSS-induced colitis in IL-6-deficient mice (Fig. 5E). Importantly, the increase of serum LRG in IL-6-deficient mice was similar to that in WT mice (Fig. 5A,E). These findings indicate that LRG expression can be induced in the absence of IL-6.

DISCUSSION

In this study we first demonstrated that serum LRG levels were significantly increased in sera of active UC patients compared with patients in remission and HC. Serum LRG is likely elevated in diverse racial groups, because we detected increased serum LRG levels not only in Japanese patients (Fig. 1A)[13] but also in Caucasian patients with UC (Fig. 1C,D) and CD (data not shown). In addition, levels of serum LRG were significantly correlated with disease activity in UC and the correlation was stronger than CRP. Moreover, by analyzing ROC curve and AUC, serum LRG levels showed higher AUC than CRP and serum LRG levels represented superior sensitivity and specificity to CRP for remission and active of UC by CAI (Fig. 2D), indicating that LRG is a useful marker to evaluate disease activity in UC. In the normal state, serum LRG is thought to be produced from liver and LRG is abundantly found in the sera of HC. In colonic inflammation, we found that the expression of LRG is increased in the inflamed mucosa of UC patients and mice with DSS colitis, suggesting that inflamed tissues can be a source for production of LRG (Fig. 3). The increased expression of LRG in inflamed tissue has previously been observed in appendix during acute appendicitis.[28] Moreover, in acute inflammatory disorders, including appendicitis and diverticulitis, increased expression of serum LRG was observed (Fig. 1A). These results indicate that the elevated expression of LRG at inflamed sites and in sera occurs in various acute and chronic inflammatory disorders. Therefore, increased serum LRG levels are not suitable for use as a specific diagnostic marker of IBD.

CRP is the most common serum marker used to evaluate disease activity in inflammatory diseases. However, serum CRP is primarily dependent on liver production induced by circulating IL-6. Compared with CD and RA, only modest to absent CRP responses are observed in UC, despite active inflammation in colon.[9] Indeed, our cohort of 82 UC patients, analyzed in this study, included five patients with normal value of CRP while having active disease (Fig. 2A). However, our study demonstrated that serum LRG levels were significantly increased in active UC patients' sera and correlated better with disease activity of UC than CRP levels (Figs. 1A, 2A). Particularly, in the group of patients with negative CRP (CRP <0.2), significant correlation was observed between serum LRG levels and CAI (Supporting Fig. 2C). Similarly, among CRP-negative patients serum LRG levels were significantly elevated in those with endoscopically active UC, compared with UC in remission (Supporting Fig. 1B). In addition, serum LRG levels were decreased after therapy (Fig. 2C), suggesting that LRG is a useful serological biomarker for evaluating disease activity and therapeutic effect in UC.

Better correlation of serum LRG levels with disease activity of UC than CRP might be explained in part by the differences in induction mechanisms between LRG and CRP. While the expression of CRP is essentially dependent on IL-6, several cytokines may compensate for the absence of elevated IL-6 in induction of LRG expression. Accordingly, expression of LRG in COLO205 cells was induced not only by IL-6 but also by TNF-α and IL-22 (Fig. 4B), all of which were increased in sera of UC patients (Fig. 4A). Expression of LRG was strongly induced by IL-22 in COLO205 cells, correlating with enhanced STAT3 (Tyr705) phosphorylation by IL-22 compared with IL-6 (data not shown). Thus, inflammatory cytokines such as TNF-α and IL-22 may mediate LRG expression in the absence of IL-6. Moreover, using DSS-induced colitis in IL-6-deficient mice we could demonstrate an IL-6-independent pathway for LRG induction (Fig. 5E). Because promoter regions of human and mouse LRG share high sequence homology and contain putative binding sites for transcription factors such as C/EBP, MZF1, and STAT,[17] it is conceivable that the similar IL-6-independent mechanisms of LRG induction are also involved in humans. Future studies are required to fully elucidate the induction mechanisms of LRG in both humans and mice.

In the three disease categories of UC based on extent of disease, serum LRG levels tended to be low in proctitis compared with extensive colitis and left-sided colitis (Fig. 1B). In addition, correlation between serum LRG levels and disease activity did not reach significance in proctitis (Fig. 2B). Although the low number of patients with active proctitis may preclude the proper evaluation of LRG levels, limited inflamed area of proctitis may also be a reason for slight increases of serum LRG levels in these patients. Given the increased production of LRG in inflamed colonic mucosa, fecal LRG might be a more sensitive disease biomarker for UC including proctitis. Optimization for the measurement of fecal LRG is currently under way in our laboratory.

This study also highlights the potential usefulness of LRG in evaluating murine colitis. Our results indicate that serum LRG levels increase as the disease progresses in a DSS-induced colitis model (Fig. 5B,C). In addition, the LRG expression is significantly upregulated in the colon with DSS-induced colitis (Fig. 5D). Thus, LRG in mice can be an objective disease activity marker for colitis models and may be useful for preclinical studies of IBD.

In conclusion, serum LRG levels reflect disease activity of UC better than CRP, especially in patients with low CRP. In the inflammatory condition, LRG is expressed in the inflamed tissue and expression of LRG is regulated by mechanisms different from that of CRP. These findings suggest that serum LRG is a novel and potential serologic biomarker for evaluating disease activity of UC.

ACKNOWLEDGMENTS

We thank T. Mizushima for provision of appendicitis and diverticulitis patients' sera, Y. Kanazawa for secretarial

assistance, and M. Urase and A. Morimoto for technical assistance.

REFERENCES

1. Nikolaus S, Schreiber S. Diagnostics of inflammatory bowel disease. *Gastroenterology*. 2007;133:1670–1689.
2. Baumgart DC, Sandborn WJ. Inflammatory bowel disease: clinical aspects and established and evolving therapies. *Lancet*. 2007;369: 1641–1657.
3. Stange EF, Travis SP, Vermeire S, et al. European evidence based consensus on the diagnosis and management of Crohn's disease: definitions and diagnosis. *Gut*. 2006;55(Suppl 1):i1–15.
4. Caprilli R, Viscido A, Latella G. Current management of severe ulcerative colitis. *Nat Clin Pract Gastroenterol Hepatol*. 2007;4:92–101.
5. Kornbluth A, Sachar DB. Ulcerative colitis practice guidelines in adults (update): American College of Gastroenterology, Practice Parameters Committee. *Am J Gastroenterol*. 2004;99:1371–1385.
6. Sands BE, Abreu MT, Ferry GD, et al. Design issues and outcomes in IBD clinical trials. *Inflamm Bowel Dis*. 2005;11(Suppl 1):S22–28.
7. Freeman HJ. Use of the Crohn's disease activity index in clinical trials of biological agents. *World J Gastroenterol*. 2008;14:4127–4130.
8. Best WR, Becktel JM, Singleton JW, et al. Development of a Crohn's disease activity index. National Cooperative Crohn's Disease Study. *Gastroenterology*. 1976;70:439–444.
9. Vermeire S, Van Assche G, Rutgeerts P. C-reactive protein as a marker for inflammatory bowel disease. *Inflamm Bowel Dis*. 2004;10: 661–665.
10. Pepys MB, Druguet M, Klass HJ, et al. Immunological studies in inflammatory bowel disease. *Ciba Found Symp* 1977:283–304.
11. Saverymuttu SH, Hodgson HJ, Chadwick VS, et al. Differing acute phase responses in Crohn's disease and ulcerative colitis. *Gut*. 1986; 27:809–813.
12. Colombel JF, Rutgeerts P, Reinisch W, et al. Early mucosal healing with infliximab is associated with improved long-term clinical outcomes in ulcerative colitis. *Gastroenterology*. 2011;141:1194–1201.
13. Serada S, Fujimoto M, Ogata A, et al. iTRAQ-based proteomic identification of leucine-rich alpha-2 glycoprotein as a novel inflammatory biomarker in autoimmune diseases. *Ann Rheum Dis*. 2010;69:770–774.
14. Haupt H, Baudner S. Isolation and characterization of an unknown, leucine-rich 3.1-S-alpha2-glycoprotein from human serum [author's transl]. *Hoppe Seylers Z Physiol Chem*. 1977;358:639–646.
15. Takahashi N, Takahashi Y, Putnam FW. Periodicity of leucine and tandem repetition of a 24-amino acid segment in the primary structure of leucine-rich alpha 2-glycoprotein of human serum. *Proc Natl Acad Sci U S A*. 1985;82:1906–1910.
16. Shirai R, Hirano F, Ohkura N, et al. Up-regulation of the expression of leucine-rich alpha(2)-glycoprotein in hepatocytes by the mediators of acute-phase response. *Biochem Biophys Res Commun*. 2009;382: 776–769.
17. O'Donnell LC, Druhan LJ, Avalos BR. Molecular characterization and expression analysis of leucine-rich alpha2-glycoprotein, a novel marker of granulocytic differentiation. *J Leukoc Biol*. 2002;72: 478–485.
18. Rachmilewitz D. Coated mesalazine (5-aminosalicylic acid) versus sulphasalazine in the treatment of active ulcerative colitis: a randomised trial. *BMJ*. 1989;298:82–86.
19. Kruis W, Schreiber S, Theuer D, et al. Low dose balsalazide (1.5 g twice daily) and mesalazine (0.5 g three times daily) maintained remission of ulcerative colitis but high dose balsalazide (3.0 g twice daily) was superior in preventing relapses. *Gut*. 2001;49:783–789.
20. Matts SG. The value of rectal biopsy in the diagnosis of ulcerative colitis. *Q J Med*. 1961;30:393–407.
21. Iwahori K, Serada S, Fujimoto M, et al. Overexpression of SOCS3 exhibits preclinical antitumor activity against malignant pleural mesothelioma. *Int J Cancer*. 2011;129:1005–1017.
22. Kim A, Enomoto T, Serada S, et al. Enhanced expression of Annexin A4 in clear cell carcinoma of the ovary and its association with chemoresistance to carboplatin. *Int J Cancer*. 2009;125:2316–2322.
23. Fujimoto M, Nakano M, Terabe F, et al. The influence of excessive IL-6 production in vivo on the development and function of Foxp3+ regulatory T cells. *J Immunol*. 2011;186:32–40.
24. Murch SH, Lamkin VA, Savage MO, et al. Serum concentrations of tumour necrosis factor alpha in childhood chronic inflammatory bowel disease. *Gut*. 1991;32:913–917.
25. Woywodt A, Ludwig D, Neustock P, et al. Mucosal cytokine expression, cellular markers and adhesion molecules in inflammatory bowel disease. *Eur J Gastroenterol Hepatol*. 1999;11:267–276.
26. Andoh A, Zhang Z, Inatomi O, et al. Interleukin-22, a member of the IL-10 subfamily, induces inflammatory responses in colonic subepithelial myofibroblasts. *Gastroenterology*. 2005;129:969–984.
27. Okayasu I, Hatakeyama S, Yamada M, et al. A novel method in the induction of reliable experimental acute and chronic ulcerative colitis in mice. *Gastroenterology*. 1990;98:694–702.
28. Kentsis A, Lin YY, Kurek K, et al. Discovery and validation of urine markers of acute pediatric appendicitis using high-accuracy mass spectrometry. *Ann Emerg Med*. 2010;55:62–70 e4.

IJC
International Journal of Cancer

Antiproliferative effect of SOCS-1 through the suppression of STAT3 and p38 MAPK activation in gastric cancer cells

Yoshihito Souma[1], Toshirou Nishida[2], Satoshi Serada[3], Kota Iwahori[3], Tsuyoshi Takahashi[4], Minoru Fujimoto[3], Barry Ripley[5], Kiyokazu Nakajima[1], Yasuaki Miyazaki[1], Masaki Mori[1], Yuichiro Doki[1], Yoshiki Sawa[1] and Tetsuji Naka[3]

[1] Department of Surgery, Osaka University Graduate School of Medicine, Osaka, Japan
[2] Department of Surgery, Osaka Police Hospital, Osaka, Japan
[3] Laboratory for Immune Signal, National Institute of Biomedical Innovation, Osaka, Japan
[4] Department of Surgery, Osaka General Medical Center, Osaka, Japan
[5] Laboratory of Immune Regulation, Osaka University Graduate School of Frontier Biosciences, Osaka, Japan

Inflammation is a crucial driving force in the development of gastric cancers (GCs). Accordingly, persistent activation of STAT3, a transcription factor pivotal in regulating both inflammation and oncogenesis, is often detected in GC, although its mechanism remains elusive. Suppressor of cytokine signaling-1 (SOCS-1) is a negative regulator of proinflammatory cytokine signaling and *SOCS-1* gene methylation is frequently detected in various cancers including GC. However, the significance of *SOCS-1* methylation in GC cells remains unexplored. Our study is undertaken to evaluate the role of SOCS-1 in GC cell proliferation and its effect on signaling pathways in GC cells. Among five GC cell lines, *SOCS-1* gene was methylated in all cell lines and constitutive STAT3 phosphorylation with elevated endogenous IL-6 production was detected in two cell lines (NUGC-3 and AGS). Unexpectedly, anti-IL-6R antibody inhibited neither cell proliferation nor STAT3 phosphorylation in NUGC-3 and AGS. In contrast, enforced SOCS-1 expression by adenoviral vector (AdSOCS-1) markedly suppressed STAT3 phosphorylation and proliferation of NUGC-3 and AGS cells *in vitro*. Interestingly, the antiproliferative effect of SOCS-1 was attributable not only to the inhibition of STAT3 but also to that of p38 MAPK activity, and chemical inhibitors of JAK/STAT and p38 MAPK signaling effectively suppressed proliferation of these GC cells. Furthermore, treatment with AdSOCS-1 *in vivo* significantly suppressed GC proliferation in a xenograft model. These results suggest that *SOCS-1* gene methylation is a critical step in the development of GC, and enforced expression of SOCS-1 may represent a novel therapeutic approach for the treatment of GC.

Gastric cancer (GC) is the second most common cause of cancer deaths worldwide.[1] Recent diagnostic and therapeutic advances have significantly improved prognosis for patients with early GC. However, an effective treatment for patients with advanced GC has not yet been established and prognosis remains poor.[2]

Key words: gastric cancer, suppressor of cytokine signaling, Janus kinase, signal transducer and activator of transcription, p38 mitogen-activated protein kinase

Abbreviations: GC: gastric cancer; IL-6R: interleukin-6 receptor; JAK: Janus kinase; p38 MAPK: p38 mitosis-activated protein kinase; SOCS: suppressor of cytokine signaling; STAT3: signal transducer and activator of transcription 3

Additional Supporting Information may be found in the online version of this article.

Grant sponsor: National Institute of Biomedical Innovation
DOI: 10.1002/ijc.27350
History: Received 12 Apr 2011; Accepted 25 Oct 2011; Online 18 Nov 2011

Correspondence to: Tetsuji Naka, Laboratory for Immune Signal, National Institute of Biomedical Innovation, 7-6-8 Saito-Asagi, Ibaraki, Osaka 567-0085, Japan, Tel.: +81-72-641-9844, Fax: +81-72-641-9837, E-mail: tnaka@nibio.go.jp

It has become evident that inflammatory responses can promote cancer development.[3] An important factor in gastric carcinogenesis is persistent inflammation in gastric epithelium due to infection of *H. pylori*.[4] Critical contributors involved in both inflammation and tumorigenesis are proinflammatory cytokines and their downstream signaling pathways. Indeed, dysregulated activation of the JAK/STAT signaling pathway, the major downstream pathway of cytokines such as IL-6, has been detected in various cancers including GC.[5–10] In particular, constitutive activation of STAT3, an important mediator of both proinflammatory and oncogenic signals of IL-6 family cytokines, is linked to inflammation-associated tumorigenesis[6–8,11] and has been detected in ~30% of primary GC.[12] In addition, activation of other signaling pathways, such as mitogen-activated protein kinase (MAPK) and phosphoinositide 3 kinase (PI3K) pathways, downstream of proinflammatory cytokines are also involved in the progression of GC.[13] However, the mechanisms for dysregulated activation of these signaling pathways in cancer cells are largely unknown.

Under homeostatic conditions, cytokine signaling pathways are tightly controlled by negative regulatory mechanisms. The most representative of these mechanisms is the induction of suppressors of cytokine signaling (SOCS) family